https://doi.org/10.1093/plcell/koac055 THE PLANT CELL 2022: 34: 1822–1843

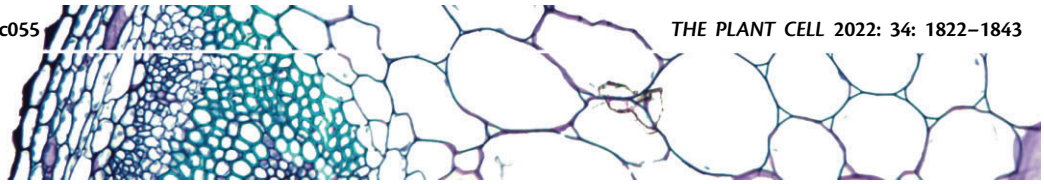

Research Article

An evolutionarily conserved C4HC3-type E3 ligase regulates plant broad-spectrum resistance against pathogens

Shuai Fu [1], Kun Wang [1], Tingting Ma [1,2], Yan Liang [1], Zhonghua Ma [1], Jianxiang Wu [1], Yi Xu [1,3] and Xueping Zhou [1,2,*,†]

1 State Key Laboratory of Rice Biology, Institute of Biotechnology, Zhejiang University, Hangzhou 310058, China
2 State Key Laboratory for Biology of Plant Diseases and Insect Pests, Institute of Plant Protection, Chinese Academy of Agricultural Sciences, Beijing 100193, China
3 Department of Plant Pathology, Nanjing Agricultural University, Nanjing 210095, China

*Author for correspondence: zzhou@zju.edu.cn
These authors contributed equally (S.F. and K.W.).
†Senior author

X.Z. and S.F. designed the experiments. S.F., K.W., and T.M. performed the experiments. X.Z., S.F., and Y.X. wrote the manuscript. X.Z., S.F., Y.X., J.W., Y.L., and Z.M. revised the manuscript.

The author responsible for distribution of materials integral to the findings presented in this article in accordance with the policy described in the Instructions for Authors (https://academic.oup.com/plcell) is: Xueping Zhou (zzhou@zju.edu.cn).

Abstract

Deployment of broad-spectrum disease resistance against multiple pathogen species is an efficient way to control plant diseases. Here, we identify a Microtubule-associated C4HC3-type E3 Ligase (MEL) in both *Nicotiana benthamiana* and *Oryza sativa*, and show that it is able to integrate and initiate a series of host immune signaling, conferring broad-spectrum resistance to viral, fungal, and bacterial pathogens. We demonstrate that MEL forms homodimer through intermolecular disulfide bonds between its cysteine residues in the SWIM domain, and interacts with its substrate serine hydroxymethyltrasferase 1 (SHMT1) through the YφNL motif. Ubiquitin ligase activity, homodimerization and YφNL motif are indispensable for MEL to regulate plant immunity by mediating SHMT1 degradation through the 26S proteasome pathway. Our findings provide a fundamental basis for utilizing the MEL–SHMT1 module to generate broad-spectrum-resistant rice to global destructive pathogens including rice stripe virus, *Magnaporthe oryzae*, and *Xanthomonas oryzae* pv. oryzae.

Introduction

Plants are exposed to a wide variety of pathogens in natural ecosystems, which can cause losses in crop yield and reduce the quality of agricultural production (Savary et al., 2019). Upon pathogen invasion, plants activate multilayered immune responses, including pathogen-associated molecular pattern (PAMP)-triggered immunity, effector-triggered immunity, ubiquitin (Ub)/26S proteasome- and autophagy-mediated turnover of pathogen-encoded proteins or immunity-related components, and RNA silencing/interference (Liu et al., 2014; Verchot, 2016; Muhammad et al., 2019; Ismayil et al., 2020). These responses include some common immune signaling systems, such as generation of reactive oxygen species (ROS), rapid intracellular activation

Received November 01, 2021. Accepted January 11, 2022. Advance access publication February 16, 2022

of mitogen-activated protein kinase (MAPK) cascades, hormone signaling, deposition of callose, and transcriptional reprogramming of defense-related genes (Meng and Zhang, 2013; Xin and He, 2013; Birkenbihl et al., 2017; Calil and Fontes, 2017). Such plant immune signaling systems are valuable targets for designing broad-spectrum resistance in crops (Senthil-Kumar and Mysore, 2013; Boutrot and Zipfel, 2017; Li et al., 2019, 2020).

Ubiquitination involves the conjugation of the Ub to a target protein and is achieved by the action of a hierarchical enzymatic cascade comprising an Ub-activating enzyme E1, an Ub-conjugating enzyme E2, and an Ub ligase E3, where the E3 Ub ligase provides substrate specificity (Verchot, 2016; Calil and Fontes, 2017). Really Interesting New Gene (RING)-type E3 ligases contain RING finger domain, which is defined by the presence of eight cysteine and histidine residues in a conserved spacing that coordinates two zinc (Zn^{2+}) ions (Stone et al., 2005; Sun et al., 2019). In addition to the two canonical RING types (C3H2C3 or C3HC4), plant RING-type E3 ligase can be subdivided into other modified (noncanonical) RING domains, including RING-v, RING-D, RING-S/T, RING-G, and RING-C2, etc. These modified RING domains varied in either the metal-ligand space or have substitutions at one or more of the metal-ligand positions (Stone et al., 2005). RING-v (also named C4HC3-type RING finger domain) is characterized by a cysteine residue at metal-ligand position 4 and a histidine residue at metal-ligand position 5 (Stone et al., 2005; Sun et al., 2019). Although a dozen plant RING-type E3 Ub ligases have been shown to play positive or negative roles during the regulation of various steps of plant immunity (Park et al., 2012; Serrano et al., 2014; Ning et al., 2015; Shen et al., 2016; Marino et al., 2019), functions of the "non-canonical" C4HC3-type RING E3 ligase in plant immunity remain elusive, and its mode of substrate recognition is unclear.

Serine hydroxymethyltransferase (SHMT), an enzyme present in all living organisms, catalyzes the reversible conversion of serine and tetrahydrofolate (THF) to glycine and 5,10-methylene THF, providing one-carbon units for the synthesis of thymidylate, purine, and methionine (Ducker and Rabinowitz, 2017). SHMT is involved in one-carbon metabolism and ROS production, which regulates cellular responses to multiple stresses, including human or plant diseases (Moreno et al., 2005; Liu et al., 2012a; Gupta et al., 2017). In plants, SHMT has paralogs that localize in different cell compartments, including cytosol, mitochondria, plastid, and nucleus (Zhang et al., 2010; Zhou et al., 2012; Liu et al., 2012a). Alteration of the regulation of cytosolic SHMT in soybean (*Glycine max*) affects one-carbon folate metabolism and improves soybean resistance to cyst nematode (Liu et al., 2012a; Korasick et al., 2020). An Arabidopsis recessive mutant in the mitochondrial SHMT1, *shmt1*, is defective in photorespiration and displays excessive accumulation of ROS, ultimately influencing responses to salt stress and pathogen infection (Moreno et al., 2005; Zhou et al., 2012). AtSHMT1 is degraded through the Ub/26S proteasome and can be stabilized by the Ub-specific protease UBP16 (Zhou et al., 2012), although the E3 ligase that triggers ubiquitination of SHMT1 is unknown. Accumulating evidence supports the importance of SHMTs in plant and human ROS regulation. However, little is known about the molecular mechanisms that regulate the activity of these enzymes. In spite of multiple broad-spectrum resistance genes that have been identified in different plant species, only a limited number of them confer species-nonspecific broad-spectrum resistance to viral, fungal and bacterial pathogens simultaneously (Quilis et al., 2008; You et al., 2016; Liu et al., 2017; Zhou et al., 2018). In this study, we show that a Microtubule-associated C4HC3-type E3 Ligase (MEL) can ubiquitinate and promote degradation of SHMT1, resulting in initiating a series of plant immune signaling that confers broad-spectrum resistance to independently evolved pathogens.

Results

NbMEL is a microtubule-associated E3 ligase and negatively regulates RSV infection

In RNA-sequencing (RNA-seq) assays using rice stripe virus (RSV)-infected and mock-inoculated (CK-) *Nicotiana benthamiana* plants at 10 days postinoculation (dpi), we found that 10 transcripts encoding E3 ligase-like proteins were significantly differentially expressed in the infected samples. Among them, eight were upregulated, and two were downregulated (Supplemental Figure S1A). Tobacco rattle virus-induced gene silencing of these transcripts followed by RSV inoculation demonstrated that knockdown of the Niben101Scf01611g03014.1 transcript remarkably enhanced RSV-induced symptom development and viral capsid protein (CP) accumulation (Supplemental Figure S1, B–D). Sequence analysis of the Niben101Scf01611g03014.1 transcript revealed an open reading frame (ORF) encoding a 242 amino acid (aa) protein comprising a SWIM Zn^{2+}-binding domain (IPR006564) in its N-terminus and a C4HC3-type RING finger domain (IPR013083) in its C-terminus (Figure 1A; Supplemental Figure S1E). We named this gene *NbMEL* based on its localization and function (see following sections). Reverse transcription-quantitative PCR (RT-qPCR) confirmed the expression of *NbMEL* increased by about four-fold at 10 dpi in RSV systemically infected leaves (Figure 1B). NbMEL is homologous to the N-terminal region of human ZSWIM2 (MAP kinase kinase kinase (MEKK1)-related protein X) and MEKK (Figure 1A; Supplemental Figure S1E), but functions of MEL homologs have not been characterized in plants.

NbMEL is expressed mainly in young leaves, flowers, and stems, whereas the lowest expression was observed in mature leaves and roots, as shown by RT-qPCR (Supplemental Figure S2A). Histochemical GUS staining of transgenic plants expressing *GUS* under the control of the *NbMEL* native promoter (*proNbMEL*) confirmed a high level of promoter activity in young leaves, shoot tips, stems, and anthers, and a low

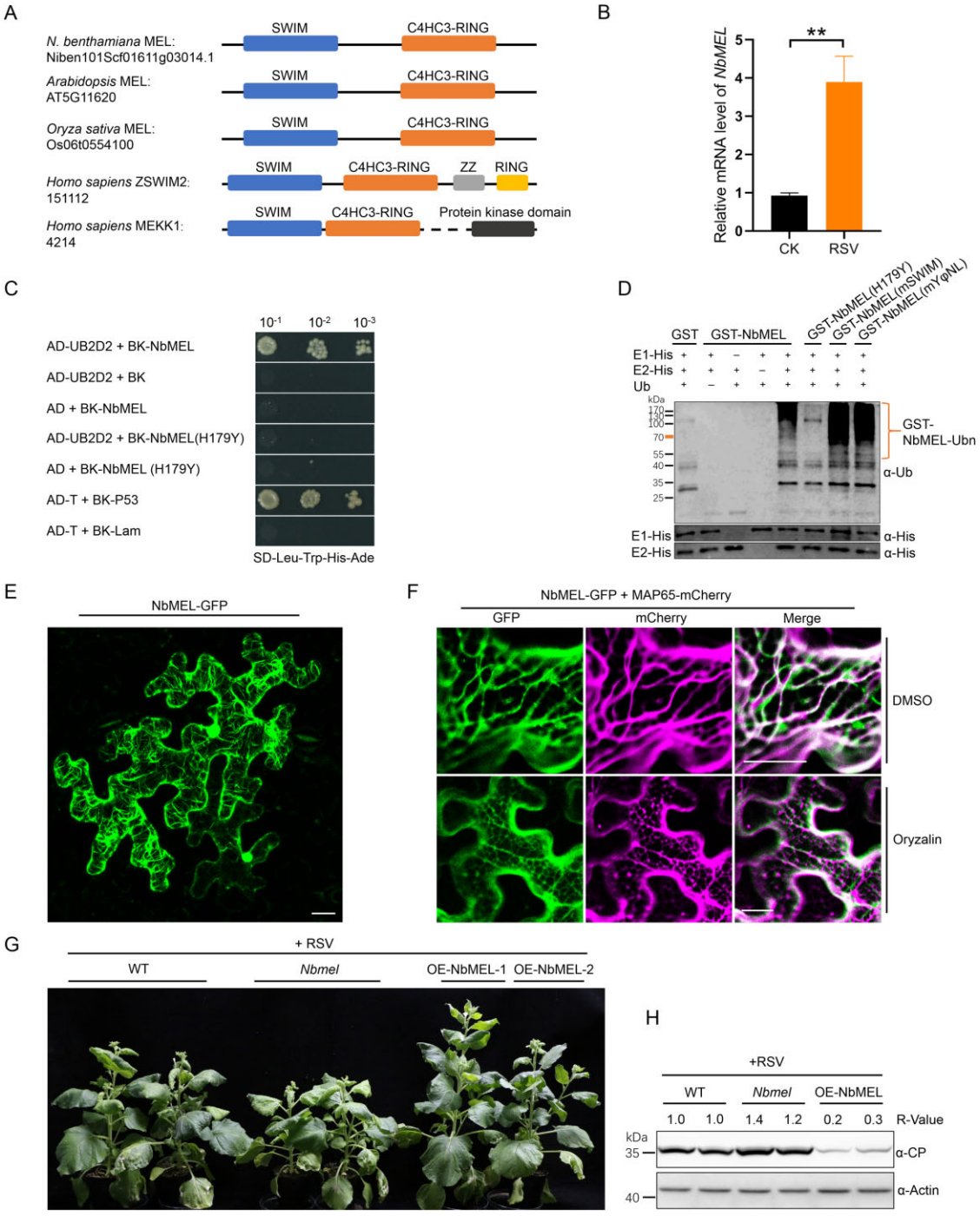

Figure 1 NbMEL is a microtubule-associated E3 ligase negatively regulating RSV infection. A, Representation of NbMEL and its homologs from Arabidopsis, *O. sativa*, and *Homo sapiens* (ZSWIM2 and MEKK1). Blue box represents SWIM domain; orange red box represents C4HC3-type RING domain; gray box represents Zn^{2+} finger domain; black box represents protein kinase domain. B, *NbMEL* transcript level in mock (CK) or RSV-infected *N. benthamiana* systemic leaves at 10 dpi detected by RT-qPCR. Data are means ± SD ($n = 3$). Asterisks mark significant differences according to two-tailed Student's *t* test, $^{**}P < 0.01$. C, NbMEL interacts with human E2 Ub-conjugating enzymes UB2D2 in Y2H assays. D, NbMEL self-ubiquitination in vitro. NbMEL and its mutants, including NbMEL(H179Y), NbMEL(mSWIM), and NbMEL(mYφNL), were assayed for self-ubiquitination in the presence of E1, human E2(UB2D2) and Ub. GST was used as a negative control. The anti-Ub antibody was used to detect ubiquitination. E, Subcellular localization of NbMEL-GFP expressed by agroinfiltration in *N. benthamiana* epidermal cells. Confocal images were taken at 48 hpi. Bar: 20 μm. F, Subcellular co-localization assay of NbMEL-GFP co-expressed with the MAP65-mCherry by agroinfiltration in *N. benthamiana* epidermal cells. Confocal images were taken at 48 hpi. Bar: 20 μm. G, Photographs of representative RSV symptoms in WT, *NbMEL* overexpressing transgenic (OE-NbMEL), and *NbMEL* knockout (*Nbmel*) *N. benthamiana* plants after 20 days postmechanical inoculated of RSV. H, RSV CP accumulation in RSV systemically infected leaves of WT, OE-NbMEL, and *Nbmel N. benthamiana* plants after 20 dpi of RSV. Actin was used as a loading control. The bands in immunoblots were quantified and the relative intensities (R-value) are shown above the band. All the experiments were performed 3 times with similar results.

level of promoter activity in mature leaves and roots (Supplemental Figure S2B). Consistent with these results, in the *proNbMEL:GUS* transgenic plants, GUS activity was strongly induced in young leaves upon RSV infection at 10 dpi (Supplemental Figure S2, C and D).

Supporting a potential function of MEL, which possesses a C4HC3-type RING domain, as an active E3 ligase, yeast two-hybrid (Y2H) assays showed that NbMEL could interact with the human E2 Ub-conjugating enzyme UB2D2, whereas an E3 ligase inactive mutant NbMEL(H179Y) in which His-179 has been replaced by Tyr in the C4HC3-type RING domain abolished this interaction (Figure 1C). In vitro self-ubiquitination assays showed that high molecular weight Ub conjugates were observed when GST-NbMEL was added, while these Ub conjugates were remarkably diminished in the case of GST-NbMEL(H179Y) (Figure 1D). These results demonstrate that NbMEL possesses E3 ligase activity, for which the C4HC3-type RING domain is essential.

To investigate the cellular distribution of NbMEL, we transiently expressed NbMEL-GFP in *N. benthamiana* leaf epidermal cells by agroinfiltration. Confocal micrographs showed that NbMEL-GFP localized in the nucleus and the cytoskeleton at the cell cortex (Figure 1E). Treatment with the microtubule-depolymerizing drug oryzalin completely abolished the co-localization of NbMEL-GFP and mCherry-tagged microtubule-associated protein 65 (MAP65-mCherry), whereas dimethyl sulfoxide (DMSO)-treated controls appeared unaffected (Figure 1F), suggesting that NbMEL is localized in microtubules.

To test the roles of NbMEL in RSV infection, NbMEL and its allele Niben101Scf01056g03007.1 (92% aa identity) were simultaneously knocked out by clustered regularly interspaced short palindromic repeats-associated protein-9 nuclease (CRISPR/Cas9)-mediated genome editing. Sanger sequencing confirmed that the NbMEL ORF was shifted by CRISPR/Cas9-mediated genome editing (Supplemental Figure S3A). The RT-qPCR analysis showed that NbMEL transcripts were also significantly decreased in *NbMEL* knockout homozygous *N. benthamiana* plants (Supplemental Figure S3B). One homozygous *NbMEL* knockout *N. benthamiana* (*Nbmel*) T1 generation plant line and two independent *NbMEL* overexpressing transgenic *N. benthamiana* T1 generation plant lines (OE-NbMEL-1 and OE-NbMEL-2) were morphologically indistinguishable from wild-type (WT) *N. benthamiana* plants under normal growth conditions (Supplemental Figure S3, C–E). Following RSV inoculation, viral symptoms and RSV CP accumulation were enhanced in *Nbmel N. benthamiana* plants and significantly attenuated in *NbMEL* overexpression *N. benthamiana* plants (Figure 1, G and H). Taken together, our results demonstrate that NbMEL is a microtubule-associated E3 ligase that has a positive function in defense against RSV infection in *N. benthamiana*.

NbMEL positively regulates plant innate immunity

Human ZSWIM2 acts as an E3 ligase and its E3 ligase activity is required for the enhancement of apoptosis, which is similar to plant hypersensitive response (HR)-like cell death. The N-terminal RING finger domain of Human MEKK1 is responsible for ubiquitination of mammal ERK1/2, and mammal ERK1/2 is closely related to plant MAP kinases (Lu et al., 2002; Nishito et al., 2006; Lord and Gunawardena, 2012; Meng and Zhang, 2013). As NbMEL is homologous to the N-terminal region of human ZSWIM2 and MEKK1, the roles of NbMEL in plant innate immunity were investigated. 3,3′-diaminobenzidine (DAB) staining indicated that agrobacterium-mediated transient expression of GFP or Ub ligase inactive mutant NbMEL(H179Y) at 36- to 48-h postinoculation (hpi) did not induce H_2O_2 accumulation, but an agrobacterium-mediated expression of NbMEL-Flag resulted in H_2O_2 accumulation in *N. benthamiana* leaves (Figure 2, A and B). By 72–96 hpi, mild HR-like cell death was observed upon expression of NbMEL-Flag and confirmed by trypan blue staining, but no obvious HR-like cell death was observed upon expression of NbMEL(H179Y)-Flag or GFP-Flag (Figure 2, A and B). Compared with GFP-Flag and NbMEL(H179Y)-Flag mutant, agrobacterium-mediated transient expression of NbMEL-Flag in *N. benthamiana* leaves led to enhanced activation of MAP kinases (Figure 2C). In transgenic *N. benthamiana* plants overexpressing *NbMEL* (OE-NbMEL), spontaneous H_2O_2 accumulation, MAP kinases as well as plant defense-related genes, including *PR2*, *PR4*, *PR5*, and *WRKY33* were constitutively activated, whereas these effects were not detected in transgenic *N. benthamiana* plants overexpressing the E3 ligase-inactive mutant (OE-NbMEL(H179Y) (Figure 2, D–G). The transcript and protein accumulations were confirmed by RT-qPCR and immunoblotting, respectively, in transgenic *N. benthamiana* plants OE-NbMEL or its mutant (Supplemental Figure S3, F and G). Interestingly, no obvious HR-like cell death was observed in constitutive *NbMEL* overexpression transgenic *N. benthamiana* plants (Supplemental Figure S3E), this might be due to NbMEL being self-ubiquitinated and the amount of NbMEL overexpression being strictly controlled in vivo.

The observed effects on MAP kinase activation, ROS generation, and increased expression of plant defense-related genes in OE-NbMEL *N. benthamiana* plants led us to investigate whether NbMEL is involved in the regulation of plant defense to pathogens other than RSV. Our histochemical GUS staining was performed in *proNbMEL:GUS* transgenic plant leaves inoculated by *Botrytis cinerea*, and GUS expression was highly induced in leaf regions surrounding lesions generated by drop inoculation of *B. cinerea* spores at 24 and 36 hpi (Supplemental Figure S4A), and RT-qPCR results revealed that the *NbMEL* transcript remarkably increased in response to infection by *B. cinerea* at 24–36 hpi (Supplemental Figure S4B). In addition, RT-qPCR results revealed that *NbMEL* transcript was not affected from 10 min to 36 h after mechanical damage (MD), excluding the possibility that *NbMEL* is induced by MD during pathogen inoculation (Supplemental Figure S4C). These results indicate that *B. cinerea* infection can also activate the transcriptional expression of *NbMEL*.

Next, OE-NbMEL, *Nbmel*, and WT *N. benthamiana* plants were challenged with *B. cinerea* or RSV. As shown in

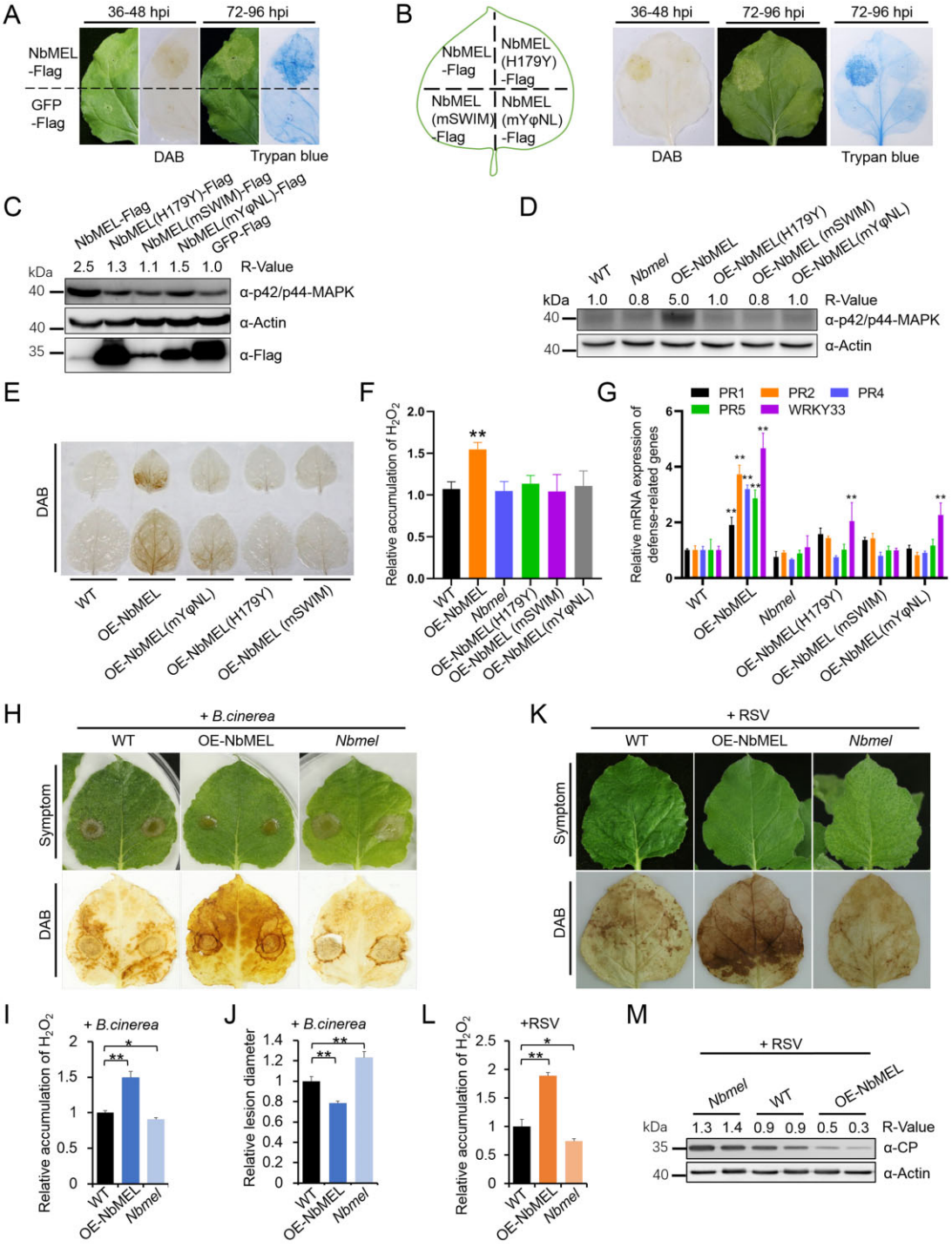

Figure 2 NbMEL positively regulates plant immunity. A and B, DAB and trypan blue staining of *N. benthamiana* leaves transiently expressing NbMEL, NbMEL mutants or GFP by agroinfiltration. DAB staining was performed at 36–48 hpi, trypan blue staining was performed at 72–96 hpi. C, MAP kinase phosphorylation detection in *N. benthamiana* leaves transiently expressing NbMEL, NbMEL mutant versions or GFP by agroinfiltration. D–G, MAP kinase phosphorylation (D), DAB staining (E), relative H_2O_2 accumulation (F), defense-related gene expression (G) in WT, *NbMEL*, or *NbMEL* mutant overexpressing transgenic (OE-NbMELs), and *NbMEL* knockout (*Nbmel*) *N. benthamiana* plants. Defense-related gene expression was detected by RT-qPCR. Data are means ± SD (n = 3). H–J, Photographs of representative lesions and DAB staining (H), relative H_2O_2 quantification (I), and relative lesion diameter (J) of *B. cinerea* conidial infected leaves of WT, OE-NbMEL, and *Nbmel N. benthamiana* plants at 96 hour post inoculation (hpi). Lesion size was measured at 3 dpi, Data are means ± SEM (n = 12). K–M, Photographs of representative symptoms and DAB staining (K), relative quantification of H_2O_2 accumulation (L), and RSV CP accumulation (M) in RSV systemically infected leaves of WT, OE-NbMEL, and *Nbmel N. benthamiana* plants after 10 dpi of RSV. In (F), (I), and (L), H_2O_2 accumulation was measured by Amplex red, Data are means ± SD (n = 3). In (C) and (D), immunoblot analysis was performed using the antibody against p42/p44-MAPK. In (F), (G), (I), (J), and (L), asterisks mark significant differences according to two-tailed Student's t test; *$P < 0.05$; **$P < 0.01$. In (C), (D), and (M), the bands in immunoblot were quantified and the relative intensities (R-value) are shown above the band, actin was used as a protein loading control. All the experiments were performed 3 times with similar results.

Figure 2, H–J, OE-NbMEL *N. benthamiana* plants developed smaller infection lesions and displayed higher H_2O_2 accumulation around the lesions, while the opposite phenotypes were found in *Nbmel N. benthamiana* plants. In addition, we also observed higher accumulation of H_2O_2 and lower CP accumulation in systemic leaves of OE-NbMEL *N. benthamiana* plants infected by RSV as compared with *Nbmel* and WT plants (Figure 2, K–M). The above results indicate that NbMEL enhances plant innate immune signaling, including activation of MAP kinases, ROS generation, and activation of defense-related genes, ultimately negatively regulating RSV or *B. cinerea* infection.

NbMEL interacts with and ubiquitinates NbSHMT1 to promote degradation of NbSHMT1

To further elucidate the molecular mechanism of NbMEL in regulating plant innate immunity, a Y2H cDNA library of *N. benthamiana* was used to search for NbMEL-interacting proteins. This screen yielded a clone of cDNA encoding SHMT with two alleles (Niben101Scf07073g02007.1 and Niben101Scf01048g00005.1 with 98.6% aa identity) in the *N. benthamiana* genome (Supplemental Figure S5, A and B). Since the proteins encoded by these two transcripts were clustered into the same clade (Group 1) with AtSHMT1 (AT4G37930) and OsSHMT1 (LOC Os03g52840.1) in the phylogenetic tree constructed by all SHMT homologs from *N. benthamiana*, Arabidopsis, and *Oryza sativa*, we hereafter refer to Niben101Scf01048g00005.1 (*NbSHMT1-1*) and Niben101Scf07073g02007.1 (*NbSHMT1-2*) as *NbSHMT1* (Supplemental Figure S5C).

To validate the interaction specificity of NbMEL and NbSHMT1, we further cloned three NbSHMT1 homologs *NbSHMT2* (Niben101Scf07116g00002.1), *NbSHMT3* (Niben101Scf07161g00011.1), and *NbSHMT4* (Niben101Scf02122g02019.1), respectively, from Groups 2, 3, and 4 in the phylogenetic tree (Supplemental Figure S5C) and then tested the interaction between NbMEL and these homologs by Y2H. The results showed that NbMEL specifically interacted only with NbSHMT1 (Figure 3A; Supplemental Figure S6A). The in vitro pull-down assay showed that GST-NbMEL could effectively pull down MBP-NbSHMT1, but not the GST control, indicating a physical interaction between NbMEL and NbSHMT1 (Figure 3B). Furthermore, bimolecular fluorescence complementation (BiFC) assays verified the in vivo NbMEL–NbSHMT1 interaction in planta, strong filiform and punctiform yellow fluorescence was observed upon co-expression of NbMEL-nYFP with NbSHMT1-cYFP or NbMEL-cYFP with NbSHMT1-nYFP, whereas no fluorescence was observed in the negative control combinations of NbMEL-nYFP and cYFP-tagged NbSHMT1 homologs (NbSHMT2, NbSHMT3, and NbSHMT4) or NbMEL-c-YFP and nYFP-tagged NbSHMT1 homologs (Supplemental Figure S6B). Immunoblots confirmed that all proteins were transiently expressed in samples (Supplemental Figure S6C).

As NbMEL is an E3 ligase and interacts with NbSHMT1, we then tested whether NbMEL can ubiquitinate NbSHMT1 and mediate its degradation through the 26S proteasome pathway. In in vitro ubiquitination assays, polyubiquitinated MBP-NbSHMT1 was detected following co-incubation with GST-NbMEL (Figure 3C). In contrast, the Ub ligase inactive mutant GST-NbMEL(H179Y) was unable to ubiquitinate MBP-NbSHMT1 (Figure 3C), indicating that NbSHMT1 is most likely a direct substrate of NbMEL. Furthermore, immunoprecipitation (IP) of NbSHMT1-Flag using anti-Flag beads showed that the polyubiquitinated forms of NbSHMT1-Flag were remarkably enhanced when NbSHMT1-Flag co-expressed with NbMEL-Myc, as compared to NbSHMT1-Flag expressed alone (Supplemental Figure S7), indicating that NbSHMT1 is polyubiquitinated by NbMEL in vivo.

To test whether NbSHMT1 is directly targeted for degradation by NbMEL, NbSHMT1-Flag was co-expressed with NbMEL in *N. benthamiana* leaves by agroinfiltration. Transient co-expression of NbMEL-Myc with NbSHMT1-Flag notably attenuated NbSHMT1-Flag protein accumulation, whereas co-expression of NbMEL(H179Y)-Myc or GFP-Myc with NbSHMT1-Flag as controls did not have any noticeable effect on NbSHMT1-Flag accumulation (Figure 3D), indicating that NbMEL directly induces NbSHMT1 degradation.

Semi-in vivo degradation assays showed that the endogenous NbSHMT1 in WT *N. benthamiana* leaf total protein extraction was degraded following incubation with ATP in immunoblot using the specific SHMT1 antibody (Figure 3, E and G; Supplemental Figure S8). This degradation was accelerated in *N. benthamiana* leaves OE-NbMEL, but remarkably reduced in *NbMEL* knockout *N. benthamiana* leaves (Figure 3, E and G). In addition, NbSHMT1 degradation in *N. benthamiana* leaves OE-NbMEL was suppressed by MG132 (Figure 3, F and G). In line with semi-in vivo results, the accumulation of endogenous SHMT1 was constitutively increased in *NbMEL* knockout (*Nbmel*) but decreased in OE-NbMEL *N. benthamiana* plants (Figure 3H). Based on these results, we conclude that NbMEL ubiquitinates NbSHMT1 and leads to its degradation by the 26S proteasome.

NbMEL-mediated downregulation of NbSHMT1 activates plant immunity

As *NbMEL* is induced by RSV or *B. cinerea* infection, and NbMEL directly ubiquitinates and promotes degradation of NbSHMT1, we reasoned that NbSHMT1 protein accumulation might be downregulated in response to RSV or *B. cinerea* infection. To test this hypothesis, we retrieved NbSHMT1 data from our previous iTRAQ-based proteomics assay in mock (CK-) and RSV infected *N. benthamiana* plants at 10 and 30 dpi (Fu et al., 2018). Eight NbSHMT1 peptides were identified by iTRAQ, and protein expression assays based on these eight peptides showed that NbSHMT1 protein accumulation was significantly reduced in RSV-infected plants at both 10 and 30 dpi (Supplemental Figure S9). Consistent with this result, the NbSHMT1 accumulation decrease at both 10 and 30 dpi in RSV-infected plants was verified by immunoblotting (Figure 4A). No

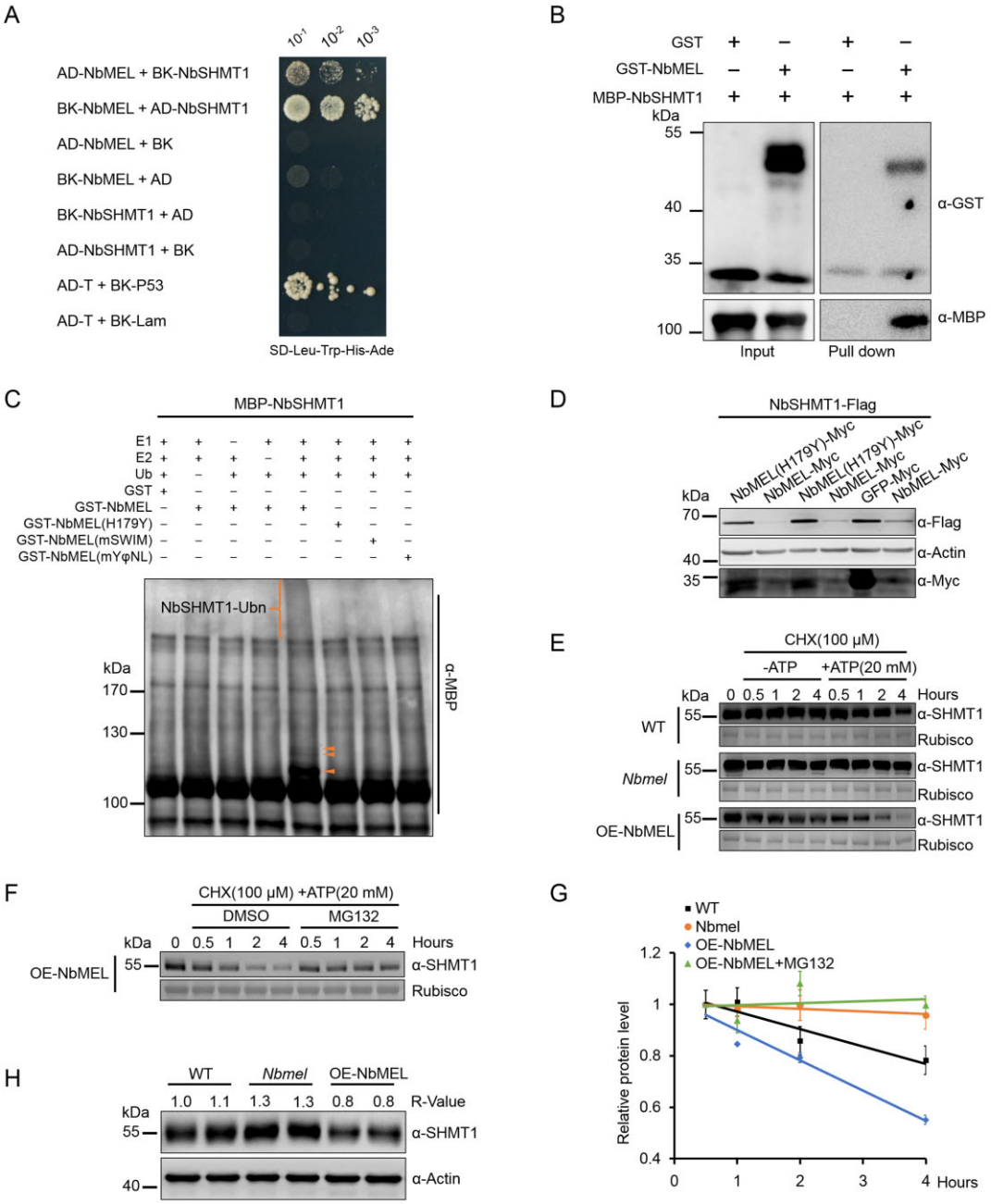

Figure 3 NbMEL interacts with and ubiquitinates NbSHMT1 to promote 26S proteasome-mediated degradation of NbSHMT1. A, NbMEL interacts with NbSHMT1 by Y2H assay. Serial dilutions of yeast cells cotransfected with two recombination vectors were plated on SD−Trp−Leu−His−Ade medium. Yeast cells co-transfected with pGADT7-T and pGBKT7-p53 or with pGADT7-T and pGBKT7-Lam were used as positive and negative controls, respectively. B, NbMEL interacts with NbSHMT1 by in vitro pull-down assay. NbMEL fused with GST (GST-NbMEL) was used as the bait, and NbSHMT1 fused with MBP was used as the prey. C, In vitro ubiquitination assay showing in vitro ubiquitination of NbSHMT1 by NbMEL and NbMEL mutants. Ubiquitination of MBP-NbSHMT1 was detected by immunoblot using the anti-MBP antibody. Orange brackets and triangles denote ubiquitinated NbSHMT1 bands. D, NbSHMT1-Flag in vivo accumulation assay. NbSHMT1-Flag was co-expressed with NbMEL, NbMEL(H179Y), or GFP (control) in *N. benthamiana* leaves by agroinfiltration. Actin was used as a loading control. E, Semi in vivo protein stability assay of endogenous NbSHMT1 in WT, *NbMEL* overexpressing transgenic (OE-NbMEL), and *NbMEL* knockout (*Nbmel*) *N. benthamiana* plants. Endogenous NbSHMT1 protein level was detected by immunoblotting with anti-SHMT1 antibody at different times (0.5, 1, 2, and 4 h) after 100-μM CHX treatment in the presence or absence of 20-μM ATP. Ponceau S staining of Rubisco was used as loading controls. F, Semi in vivo protein stability assay of the effect of MG132 on the stability of endogenous NbSHMT1 in OE-NbMEL *N. benthamiana* plants. Endogenous NbSHMT1 protein level was detected at different times (0.5, 1, 2, and 4 h) after 100-μM CHX and 20-μM ATP treatment in the presence of 100-μM MG132 or an equal volume of DMSO (control). Ponceau S staining of Rubisco was used as loading controls. G, Graph summarized relative endogenous NbSHMT1 accumulation level in (E) and (F). Protein accumulation at the 0.5-h time point was normalized to rubisco and set as 1. Data are means ± SEM (n = 3). H, Endogenous SHMT1 protein accumulation in WT, OE-NbMEL and *Nbmel N. benthamiana* plants. Actin was used as a loading control. All the experiments were performed 3 times with similar results.

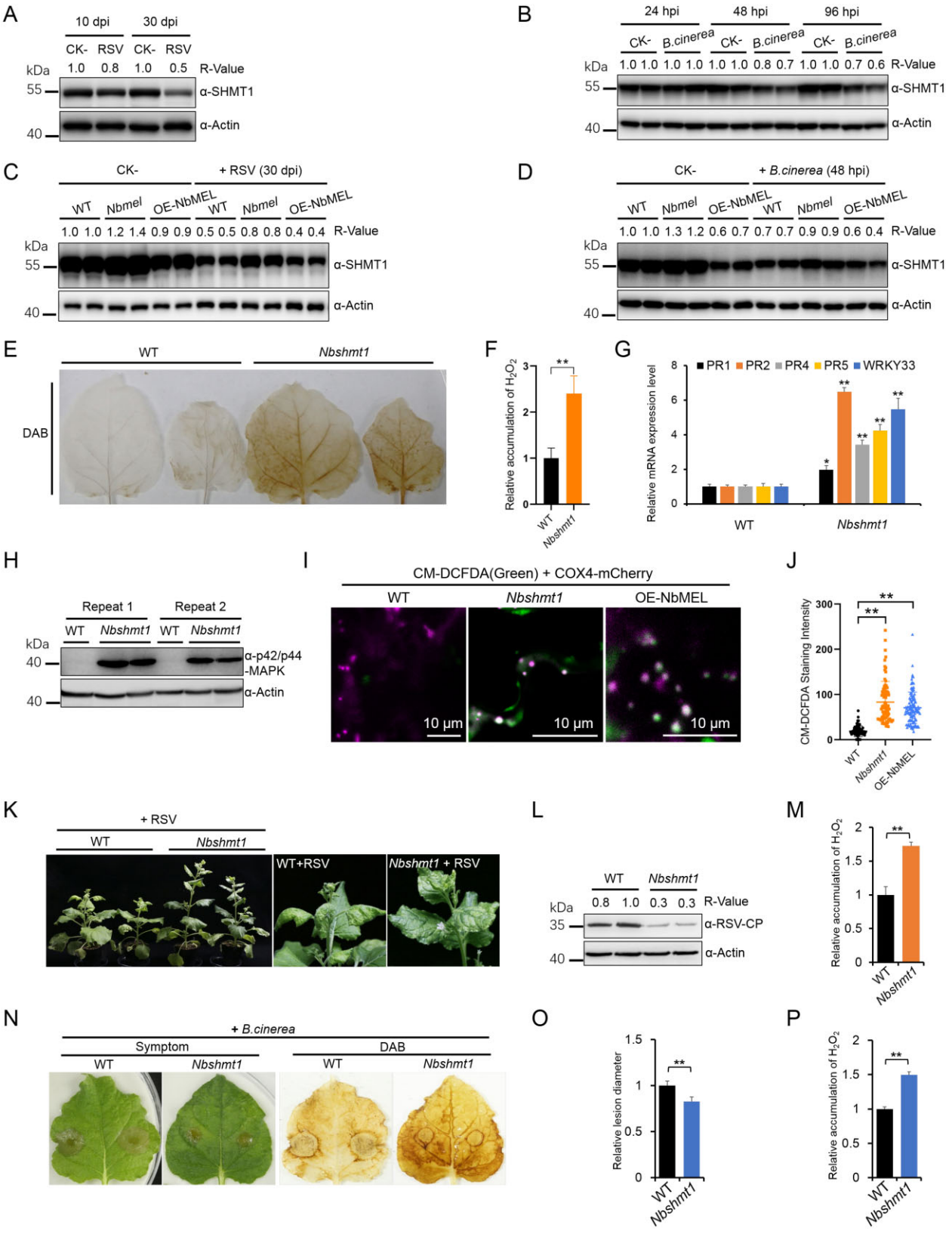

Figure 4 Downregulation of NbSHMT1 mediated by NbMEL initiates plant immune signaling. A, Endogenous NbSHMT1 accumulation in mock (CK-) and RSV-infected *N. benthamiana* systemic leaves at 10 dpi and 30 dpi, respectively. Actin was used as a loading control. B, Endogenous NbSHMT1 accumulation in mock (CK-) and *B. cinerea* infected *N. benthamiana* leaves at 24, 48, and 96 hpi, respectively. Actin was used as a loading control. C, Endogenous NbSHMT1 accumulation in mock (CK-) and RSV infected WT, *NbMEL* overexpressing transgenic (OE-NbMEL), and *NbMEL* knockout (*Nbmel*) *N. benthamiana* plants at 30 dpi. Actin was used as a loading control. D, Endogenous NbSHMT1 accumulation in mock (CK-) and *B. cinerea* infected WT, OE-NbMEL, and *Nbmel N. benthamiana* plants at 48 hpi. Actin was used as a loading control. E, DAB staining of

remarkable difference of the *NbSHMT1* transcript levels was found between mock (CK-) and RSV infected *N. benthamiana* plants when analyzed by RT-qPCR at both 10 and 30 dpi (Supplemental Figure S10A), indicating that RSV infection does not affect *NbSHMT1* transcription. Similarly, the endogenous NbSHMT1 protein level was decreased after *B. cinerea* infection from 48 hpi (Figure 4B). The RT-qPCR analysis showed that the *NbSHMT1* transcript levels were downregulated after *B. cinerea* infection from 24 hpi (Supplemental Figure S10B). These data indicate that RSV or *B. cinerea* infection induces downregulation of NbSHMT1. To address whether RSV or *B. cinerea* infection-induced degradation of NbSHMT1 is dependent on NbMEL, we compared the accumulation of NbSHMT1 in OE-NbMEL, *Nbmel* and WT plants under pathogen infection. The RSV or *B. cinerea* infection-induced NbSHMT1 degradation was much lower in *Nbmel* plants than that in WT or OE-NbMEL plants (Figure 4, C and D). These data support that NbMEL is involved in RSV or *B. cinerea* infection-induced degradation of NbSHMT1.

To investigate the role of NbSHMT1 degradation, *NbSHMT1* was knocked out by CRISPR/Cas9-mediated genome editing. Sanger sequencing confirmed CRISPR/Cas9-mediated genome mutation in NbSHMT1 ORF (Supplemental Figure S11A). The RT-qPCR and immunoblotting analyses showed that NbSHMT1 transcript and protein were also significantly decreased in *NbSHMT1* knockout homozygous *N. benthamiana* leaves (Supplemental Figures S8C and S11B). T1 generation of *NbSHMT1* knockout homozygous *N. benthamiana* leaves (*Nbshmt1*) displayed mild chlorosis under normal light intensity (4000 Lux) (Supplemental Figure S11C). When grown under high light intensity (7,000 Lux) or longer photoperiod (18-h light/6-h dark), these plants showed slightly reduced size and growth retardation, and some upper leaves presented chlorosis (Supplemental Figure S11, C and D). Mutation of Arabidopsis SHMT1 resulted in excessive accumulation of ROS (Moreno et al., 2005). DAB staining and H_2O_2 accumulation detection revealed that H_2O_2 spontaneously accumulated in *Nbshmt1* leaves (Figure 4, E and F). Similar to *NbMEL* overexpression in *N. benthamiana*, *Nbshmt1 N. benthamiana* plants displayed constitutive activation of MAP kinases and induction of defense-related genes, including *PR1*, *PR2*, *PR4*, *PR5*, and *WRKY33* (Figure 4, G and H).

AtSHMT1 was reported to localize to mitochondria (Zhou et al., 2012), and MitoProtII prediction showed NbSHMT1 was targeted to mitochondria due to the presence of an 18 aa mitochondrial targeting signal at its N-terminus. To test the predicted mitochondrial localization of NbSHMT1, NbSHMT1-GFP was transiently co-expressed with a mitochondrial marker (COX4-mCherry) in *N. benthamiana* leaves. Confocal microscopy observation demonstrated that NbSHMT1-GFP co-localized with COX4-mCherry in mitochondria (Supplemental Figure S12A). MitoTracker Red has been widely used to label mitochondria (Todisco et al., 2006). The co-localization assay showed that NbSHMT1-GFP punctate fluorescence is specifically located in the mitochondria labeled by MitoTracker Red (Supplemental Figure S12B). In immune-gold labeling transmission electron microscopy analysis, compared with GFP, NbSHMT1-GFP was distinctly labeled in mitochondria by the specific antibody against GFP, and the number of gold particles labeled in mitochondria was significantly larger in cells transiently expressing NbSHMT1-GFP than that in those expressing GFP (Supplemental Figure S12, C and D). Furthermore, the predicted NbSHMT1 mitochondrial targeting signal 1–18 aa was fused to GFP, and we found NbSHMT1 (1–18 aa)-GFP co-localized with COX4-mCherry at mitochondria (Supplemental Figure S12E), indicating that the region comprising 1–18 aa is responsible for NbSHMT1 protein targeting to mitochondria.

We then examined whether the decrease of SHMT1 could induce mitochondrion-derived ROS production in OE-NbMEL and *Nbshmt1 N. benthamiana* plants. CM-DCFDA (chloromethyl-2′, 7′-dichlorodihydrofluorescein diacetate) is a cell-permeant reagent that can react with ROS and is used to assess the oxidant levels within the cell (Shang-Guan et al., 2018). CM-DCFDA staining showed green punctiform fluorescence co-localized with the mitochondrial marker COX4-mCherry in OE-NbMEL and *Nbshmt1 N. benthamiana* leaf epidermal cells while no green fluorescence was observed in WT *N. benthamiana* leaf epidermal cells (Figure 4,

Figure 4 (Continued)
WT and *Nbshmt1 N. benthamiana* leaves. F, Relative H_2O_2 accumulation in WT and *Nbshmt1 N. benthamiana* leaves was measured by Amplex red. G, Defense-related gene expression in WT and *Nbshmt1 N. benthamiana* plants detected by RT-qPCR. Data are means ± SD (n = 3). H, MAP kinase phosphorylation assay in WT and *Nbshmt1 N. benthamiana* leaves. Immunoblot analysis was performed using an anti p42/p44-MAPK antibody. Actin was used as a loading control. I, Photographs of representative CM-H2DCFDA staining in mitochondria of WT, OE-NbMEL and *Nbshmt1 N. benthamiana* leaf epidermal cells. Bar: 10 μm. J, Comparison of fluorescence intensity of mtROS stained by CM-H2DCFDA in WT, OE-NbMEL, and *Nbshmt1 N. benthamiana* leaf epidermal cells. COX4-mCherry was used as a mitochondrial marker. Bar: 10 μm. Data are means ± SD (n = 100). K, Photographs of representative RSV symptoms in WT and *Nbshmt1 N. benthamiana* plants at 20 dpi. L and M, RSV CP accumulation (L) and relative quantification of H_2O_2 accumulation (M) in RSV-infected systemically leaves of WT and *Nbshmt1 N. benthamiana* plants at 20 dpi. Actin was used as a loading control. N–P, Photographs of representative lesions and DAB staining (N), relative lesion diameter (O), and relative quantification of H_2O_2 (P) of *B. cinerea*-infected leaves of WT and *Nbshmt1 N. benthamiana* plants at 96 hpi. Lesion size was measured at 3 dpi, Data are means ± SEM (n = 10). In (F), (M), and (P), H_2O_2 accumulation was measured by Amplex red. Data are means ± SD (n = 3). In (F), (G), (J), (M), (O), and (P), asterisks mark significant differences according to two-tailed Student's t test, $^{**}P < 0.01$. In (A–D) and (L), the bands in immunoblots were quantified and the relative intensities (R-value) are shown above the band. All the experiments were performed 3 times with similar results.

I and J), indicating that *NbMEL* overexpression or *NbSHMT1* knockout-caused intracellular ROS generation is closely associated with mitochondria. Voltage-dependent anion-selective channel protein 1–5 (VDAC1) accumulation detection indicated the number and integrity of mitochondria were not affected by *NbMEL* overexpression or *NbSHMT1* knockout (Supplemental Figure S13).

To test whether NbSHMT1 plays a role in plant immunity, *Nbshmt1* plants were inoculated with RSV or *B. cinerea*. As shown in Figure 4, K–M, both RSV-induced symptoms and accumulation of the viral CP were significantly attenuated in *Nbshmt1 N. benthamiana* plants, and higher H_2O_2 accumulation was detected in *Nbshmt1 N. benthamiana* plants infected with RSV, compared to that in WT *N. benthamiana* plants. Meanwhile, *B. cinerea* inoculation showed that *B. cinerea*-induced lesions in *Nbshmt1 N. benthamiana* plants were smaller and H_2O_2 accumulated higher around the lesions, compared to that in WT *N. benthamiana* plants (Figure 4, N–P). These results indicate that NbMEL-mediated downregulation of NbSHMT1 activates plant immunity including spontaneous mitochondrial ROS (mtROS) accumulation, activation of MAPK cascades, and defense-related genes.

NbMEL recognizes NbSHMT1 through its C-terminal YφNL motif

To investigate the molecular basis underpinning the interaction between MEL and SHMT1, Y2H assays were used to analyze the interaction between different NbMEL truncated forms with NbSHMT1 (Figure 5A). As shown in Figure 5B, the C-terminus of NbMEL (207–242 aa), but not other domains, strongly interacted with NbSHMT1. For example, the Ub ligase inactive mutant NbMEL(H179Y) was still able to interact with NbSHMT1 (Figure 5C). Interestingly, the C-terminus (207–242 aa) of NbMEL is predicted to contain an intrinsically disordered domain by DISOPRED 3 (http://bioinf.cs.ucl.ac.uk/psipred/) (Figure 5A). Next, we further narrowed down the minimal domain of NbMEL that is required for NbMEL binding of NbSHMT1 and found that the C-terminal 23 residues located at positions 207–229 were still capable to interact with NbSHMT1 (Figure 5B).

Then, we retrieved and aligned this 23-residues region of NbMEL homologs from 17 dicots, 7 monocots, 4 algae, and ferns. Strong conservation was observed for a tyrosine (Tyr) residue at position 216, a hydrophobic residue (Leu/Met/Val/Ile) at 217, an asparagine (Asn) residue at 218, and a leucine (Leu) residue at 219 (Figure 5D). We hereafter refer to this region as the YφNL motif, where φ represents a hydrophobic residue. The high sequence conservation of the NbMEL YφNL motif prompted us to determine whether the YφNL motif is required for NbSHMT1 recognition. We substituted Tyr-216, Leu-217, Asn-218, and Leu-219, to Ala simultaneously to generate a NbMEL(mYφNL) mutant, and then tested its interaction with NbSHMT1. The result showed that NbMEL(mYφNL) lost its interaction with NbSHMT1 in both Y2H (Figure 5B) and BiFC (Supplemental Figure S14A). We further showed that NbMEL(mYφNL) lost its ability to ubiquitinate MBP-NbSHMT1 in vitro (Figure 3C), while self-ubiquitination of GST-NbMEL(mYφNL) was not affected (Figure 1D). Consistent with those results, in the NbSHMT1-Flag accumulation assay, co-expression with NbMEL remarkably reduced NbSHMT1-Flag accumulation, but NbMEL(mYφNL) and GFP were unable to target NbSHMT1 for degradation (Figure 5E). Moreover, *N. benthamiana* leaves transiently expressing NbMEL(mYφNL)-Flag by Agrobacterium infiltration displayed remarkably attenuated H_2O_2 generation, MAP kinase activation, and HR-like cell death compared to those expressing NbMEL-Flag (Figure 2, B and C). In line with NbMEL(mYφNL)-Flag transient expression results, MAP kinase activation, H_2O_2 generation, and expression of defense-related genes in transgenic *N. benthamiana* plants overexpression *NbMEL (mYφNL)-Flag* (Supplemental Figure S15, A and B) were indistinguishable from those in non-transgenic plants (Figure 2, D–G). These results suggest that the conserved YφNL motif embedded in the NbMEL C-terminal intrinsically disordered region is responsible for binding with NbSHMT1 and indispensable for the NbMEL-mediated modulation of plant immune signaling.

NbMEL forms homodimers through intermolecular disulfide bonds

In Y2H assays, we found that NbMEL can strongly self-interact (Figure 5F), indicating that NbMEL might form oligomer. We further showed that the Ub ligase inactive mutant NbMEL(H179Y) and the YφNL motif mutant NbMEL(mYφNL) are still capable of self-interacting (Figure 5F), indicating that the YφNL motif and Ub-ligase activity domain are not required for NbMEL oligomerization. Then, a series of NbMEL truncated mutants were constructed to identify the domains required for NbMEL oligomerization. As shown in Figure 5F, we found that NbMEL (1–90 aa), harboring the SWIM domain, was sufficient to mediate self-interaction. A close look into the sequence of the SWIM domain unveiled that it comprises a characteristic sequence motif $CxCx_nCxH$, conserved in all plant species analyzed (Supplemental Figure S16A). Point mutations were generated in this region at positions Cys-70, Cys-72, and Cys-79 by replacing these cysteine residues with Ala, simultaneously, generating the NbMEL(m1-90 aa) mutant. Y2H results indicated that NbMEL(m1-90 aa) loses the ability to self-interact (Figure 5F). When these mutations were introduced in the full-length NbMEL, the resulting NbMEL(mSWIM) mutant also abolished self-interaction in Y2H (Figure 5F) and BiFC assays (Supplemental Figure S14B).

To test whether NbMEL could form oligomer in vivo, NbMEL(H179Y)-Flag or NbMEL(mSWIM)-Flag was Agrobacterium-mediated transiently expressed in *N. benthamiana* leaves. As shown in Figure 5G, a high molecular mass band of approximately twice the size of that of the NbMEL(H179Y)-Flag monomer was observed upon expression of NbMEL(H179Y), indicating that NbMEL(H179Y)

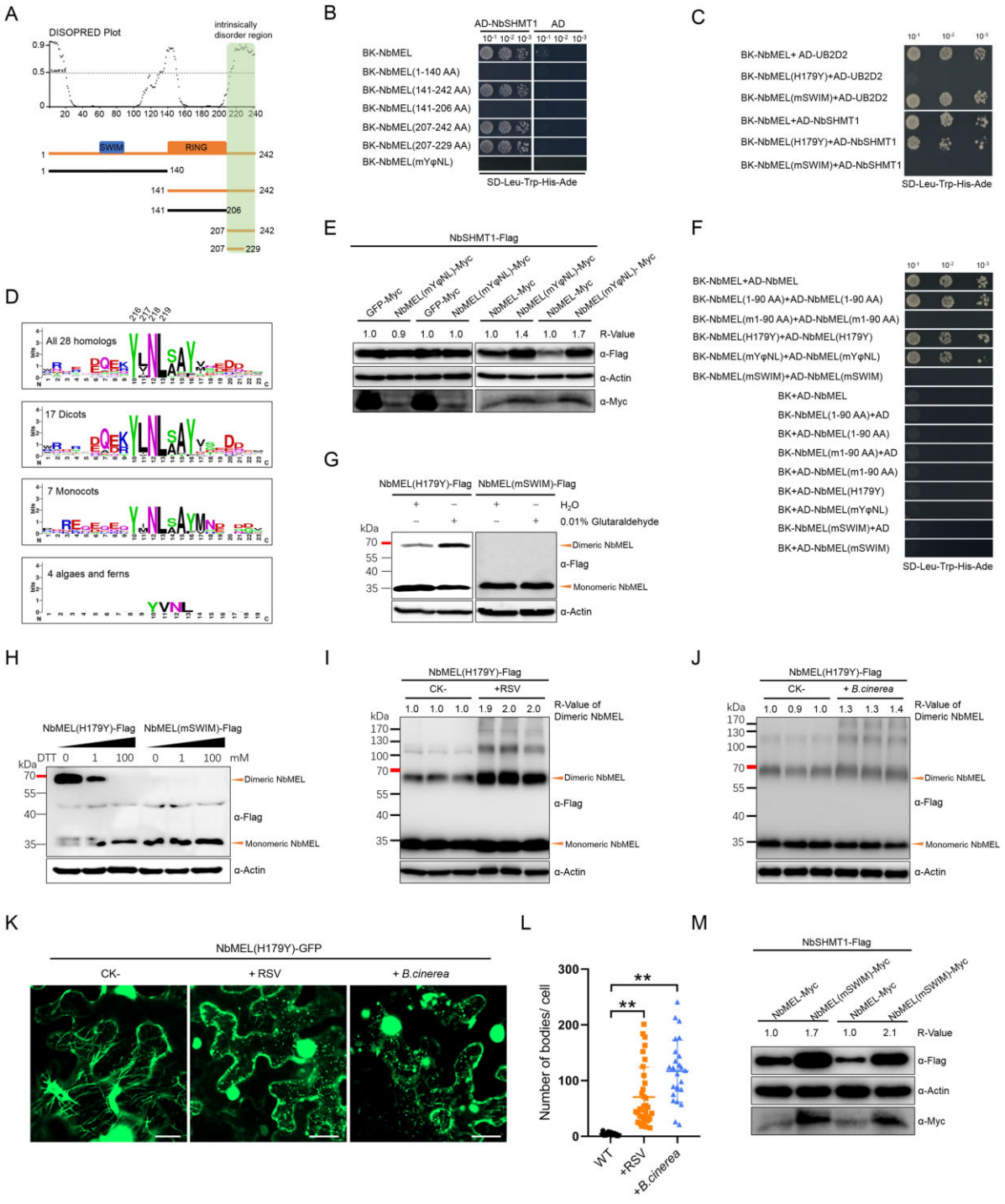

Figure 5 NbMEL recognizes NbSHMT1 through the YφNL motif and forms homodimers dependent on the SWIM domain. A, Intrinsically disordered region in NbMEL predicted by DISOPRED 3 and schematic representation of NbMEL truncated mutants. Green box indicates the NbMEL C-terminal intrinsically disordered region interacting with NbSHMT1. Black thick lines represent mutants that are unable to interact with NbSHMT1; orange thick lines represent mutants that are able to interact with substrates. B, Interaction of NbMEL, its truncated or point mutants with NbSHMT1 tested by Y2H assay. C, Interaction of NbMEL, NbMEL(mSWIM), NbMEL(H179Y) with NbSHMT1 or UB2D2 tested by Y2H assay. D, Sequence conservation of NbMEL C-terminal 23 aa region constructed from 28 MEL homologs and drawn by WebLogo. E, NbSHMT1-Flag in vivo accumulation assay when it was co-expressed with NbMEL, NbMEL(mYφNL) or GFP (control) by agroinfiltration in *N. benthamiana* leaves. Actin was used as a loading control. F, Y2H assay detection of the self-interaction of NbMEL, its truncated or point mutants. G, Agrobacterium-mediated expressed NbMEL(H179Y)-Flag forms homodimer but that of NbMEL(mSWIM)-Flag was in monomeric form in vivo. Orange triangles indicate the homodimeric or monomeric forms of NbMEL. The chemical cross-linker glutaraldehyde (0.01%) was infiltrated to *N. benthamiana* leaves 2 h before samples were harvested. Actin was used as a loading control. H, The reducing agent DTT breaks homodimerization of NbMEL(H179Y)-Flag expressed by agroinfiltration in *N. benthamiana* leaves. The supernatant of total protein extracts was treated with

forms a homodimer. Glutaraldehyde works as a crosslinker that covalently binds to oligomers and stabilizes its structure (Cubillos-Rojas et al., 2016). The dimer form of NbMEL(H179Y)-Flag was significantly increased in sample leaves preinfiltrated with 0.01% glutaraldehyde 2 h before total protein extraction, whereas only the band corresponding to the monomeric form was observed for NbMEL(mSWIM)-Flag (Figure 5G). These results suggest that NbMEL can form homodimer in vivo. Moreover, increasing amounts of reducing agent Dithiothreitol (DTT) from 0 to 100 mM led to the shift of NbMEL(H179Y)-Flag from its dimeric to its monomeric form (Figure 5H), suggesting that NbMEL homodimerization depends on the formation of intermolecular disulfide bonds. Taken together, these results strongly suggest that conserved cysteine residues in the SWIM domain contribute to the homodimerization of NbMEL.

Next, we want to know whether NbMEL forms dimer during pathogen infection. As E3 ligase inactive mutant NbMEL(H179Y) is more stable, we tested NbMEL(H179Y)-Flag accumulation during RSV or *B. cinerea* infection. NbMEL(H179Y)-Flag accumulation was detected in pathogen-infected *N. benthamiana* leaves. Dimerization of NbMEL(H179Y)-Flag was remarkably increased when NbMEL(H179Y)-Flag was transiently expressed in RSV-infected leaves as compared with that in mock (CK-) leaves (Figure 5I). In addition, we inoculated *B. cinerea* spores in leaves that had transiently expressed NbMEL(H179Y)-Flag, we found NbMEL(H179Y)-Flag converted from monomeric to dimeric after *B. cinerea* infection at 48 hpi (Figure 5J). Bands migrating above 100 kDa were also observed (Figure 5, I and J), these bands might be multimerized form of NbMEL(H179Y)-Flag. We then monitored NbMEL (H179Y)-GFP localization in pathogen-infected *N. benthamiana* leaves. We found microtubule-localized NbMEL (H179Y)-GFP was mainly localized in cytoplasmic discrete fluorescence bodies in RSV-infected *N. benthamiana* leaf epidermal cells (Figure 5, K and L). In NbMEL(H179Y)-GFP transiently expressed *N. benthamiana* leaves 48-h post *B. cinerea* inoculation, the formation of discrete NbMEL(H179Y)-GFP bodies was observed in the cytoplasm (Figure 5, K and L). These results indicate that NbMEL locates on cytoplasm discrete bodies during RSV or *B. cinerea* infection and forms a homodimer in response to RSV or *B. cinerea* infection.

We next aimed to understand if NbMEL homodimerization has biological functions. In Y2H assays, NbMEL(mSWIM) interacted with the human E2 Ub-conjugating enzyme UB2D2 but lost the ability to interact with NbSHMT1 (Figure 5C). BiFC assays also showed that NbMEL(mSWIM) lost its interaction with NbSHMT1 (Supplemental Figure S14A). These results suggest that homodimerization of NbMEL is indispensable for the interaction with NbSHMT1. An in vitro ubiquitination assay showed that GST-NbMEL(mSWIM) retains the capacity to self-ubiquitinate (Figure 1D) but loses the ability to ubiquitinate MBP-NbSHMT1 (Figure 3C). Compared to co-expression with NbMEL-Myc, NbSHMT1 protein was more stable when co-expressed with NbMEL(mSWIM)-Myc in *N. benthamiana* plants (Figure 5M), indicating that the monomeric NbMEL(mSWIM) was unable to ubiquitinate the substrate NbSHMT1 for 26S proteasome-mediated degradation. Moreover, agrobacterium-mediated transient expression of NbMEL(mSWIM)-Flag did not trigger H_2O_2 generation, MAP kinase activation, and HR-like cell death (Figure 2, B and C). Consistent with these results, in NbMEL(mSWIM)-Flag-overexpressing transgenic *N. benthamiana* plants (Supplemental Figure S15, C and D), MAP kinase activation, H_2O_2 generation, and expression of defense-related genes were comparable to those in WT plants (Figure 2, D–G). These results revealed that MEL forms homodimers through intermolecular disulfide bonds dependent on three-cysteine aa localized in the SWIM domain, and homodimerization is essential for NbMEL to positively regulate plant immunity.

The MEL–SHMT1 module is an evolutionarily conserved regulator of plant broad-spectrum disease resistance

To assess if the MEL–SHMT1 module-mediated regulation of plant immunity is conserved in other plant species, we investigated the functions of this protein module in *O. sativa*. Phylogenetic analysis and protein alignment evidenced that MEL is evolutionarily conserved in plants (Supplemental Figure S16, A and B). Rice MEL (*OsMEL*, LOC_Os06g36030.1) was cloned and subcellular localization assay showed that OsMEL-GFP co-localized with the microtubule marker MAP65-mCherry, which was abolished by oryzalin treatment (Supplemental Figure S17A). OsSHMT1 (LOC_Os03g52840.1) localized to mitochondria as indicated by co-localization with mitochondrial marker COX4-mCherry (Supplemental Figure S17B).

Similar to NbMEL, OsMEL could interact with human UB2D2 in yeast, whereas a mutant in which His-196 has been replaced with Tyr in the C4HC3-type RING domain

Figure 5 (Continued)
0–100 mM DTT at 25°C for 20 min. Black triangles above the band indicate increasing amounts of reducing agent DTT from 0 to 100 mM. Orange triangles indicate the dimeric or monomeric form of NbMEL(H179Y). I, In vivo accumulation assay of NbMEL(H179Y)-Flag expressed by agroinfiltration in mock (CK-) or RSV-infected *N. benthamiana* leaves. J, In vivo accumulation assay of NbMEL(H179Y)-Flag expressed by agroinfiltration in mock (CK-) or *B. cinerea* infected *N. benthamiana* leaves. K, Subcellular localization of NbMEL(H179Y)-GFP expressed by agroinfiltration in mock (CK-), RSV infected and *B. cinerea* inoculated *N. benthamiana* leaves. Confocal images were taken at 48 hpi. Bar: 20 μm. L, Number of NbMEL(H179Y)-GFP fluorescence bodies in mock, RSV infected and *B. cinerea* inoculated *N. benthamiana* epidermal cells. Data are means ± SD (n = 25). Asterisks mark significant differences according to two-tailed Student's t test, $^{**}P < 0.01$. In (E) and (I–J), the bands in immunoblot were quantified and the relative intensities (R-value) are shown above the band. M, NbSHMT1-Flag in vivo accumulation assay when it was co-expressed with NbMEL or NbMEL(mSWIM) by agroinfiltration in *N. benthamiana* leaves. Actin was used as a loading control. All the experiments were performed 3 times with similar results.

could not (Supplemental Figure S18A). In the in vitro self-ubiquitination assay, high molecular weight Ub conjugates were observed for GST-OsMEL, but not for GST-OsMEL(H196Y) (Supplemental Figure S18B). The interaction of OsMEL and OsSHMT1 was also validated by both Y2H and BiFC assays (Supplemental Figure S18, C and D). Self-interaction of OsMEL or OsSHMT1 in BiFC indicated all proteins used in BiFC had expressed in vivo (Supplemental Figure S18D). Moreover, polyubiquitinated MBP-OsSHMT1 could be detected when MBP-OsSHMT1 was co-incubated with GST-OsMEL in the in vitro ubiquitination assay; in contrast, the Ub ligase-inactive mutant GST-OsMEL(H196Y) could not ubiquitinate MBP-OsSHMT1 (Supplemental Figure S18E). Furthermore, Agrobacterium-mediated transient co-expression of OsMEL-Flag with OsSHMT1-GFP remarkably reduced the accumulation of OsSHMT-GFP in *N. benthamiana* leaves (Supplemental Figure S18F). Therefore, OsSHMT1 is a direct substrate of OsMEL.

Next, *OsMEL* overexpressing transgenic (OE-OsMEL-25/34) and *OsMEL* knockout (*Osmel*) *O. sativa* (Cultivar ZH11) plant lines were generated (Supplemental Figure S19, A and B). Sanger sequencing confirmed CRISPR/Cas9-mediated genome mutation in OsMEL ORF (Supplemental Figure S19A). Importantly, OsSHMT1 accumulated to higher levels in T1 generation of *Osmel O. sativa* plants but to remarkable lower levels in the T1 generation of *OsMEL*-overexpressing *O. sativa* plants when compared to WT *O. sativa* plants (Supplemental Figure S19C). Our results indicate that MEL ubiquitinates and controls the steady-state level of SHMT1 in a system that is highly conserved in plants.

We observed that OE-OsMEL *O. sativa* plants displayed smaller in plant size compared with *Osmel* and WT *O. sativa* plants (Figure 6A). Besides, H_2O_2 accumulation was higher in OsMEL overexpressing transgenic *O. sativa* leaves than that in *Osmel* and WT *O. sativa* leaves (Supplemental Figure S19, D and E). In addition, defense-related genes were remarkably induced in OE-OsMEL *O. sativa* plants but suppressed in *Osmel O. sativa* plants (Supplemental Figure S19F). *Oryza sativa* plants overexpressing OsMEL phenocopied the homozygous *OsSHMT1* knockout *O. sativa* (*Osshmt1*) plants, but *Osshmt1* plants showed more severe chlorosis, dwarfism, and ultimately lethality concomitant to massive accumulation of H_2O_2, as demonstrated by DAB staining (Supplemental Figure S20, A–C). In parallel, defense-related genes were remarkably suppressed in transgenic rice overexpressing *OsSHMT1* (OE-OsSHMT-8/10) (Supplemental Figure S20, D and E).

As plant immunity signaling was activated in OE-OsMEL and suppressed in *Osmel* and OE-OsSHMT1 rice, we asked whether the OsMEL–OsSHMT1 module could regulate *O. sativa* innate immunity against invading multiple pathogens. Interestingly, as previously observed in *N. benthamiana*, we found that the OsSHMT1 protein accumulation was also prominently reduced in response to RSV, *Magnaporthe oryzae*, or *Xanthomonas oryzae* pv. oryzae (*Xoo*) infection on *O. sativa* (Supplemental Figure S21). RSV inoculation by RSV-viruliferous small brown plant hopper (*Laodelphax striatellus*) revealed that overexpression of *OsMEL* in *O. sativa* (OE-OsMEL-25/34) attenuated RSV-triggered symptoms (Figure 6, A and B), concomitant to lower accumulation of the RSV CP (Figure 6C). On the contrary, *Osmel* plants displayed more severe stunting and symptom severity upon RSV infection (Figure 6, A and B), accompanied by a higher accumulation of the RSV CP (Figure 6C). Similar to *Osmel* plants, RSV infection on OE-OsSHMT1 *O. sativa* plants (OE-OsSHMT-8/10) displayed more severe stunting and symptom severity (Figure 6, D and E), accompanied by enhanced accumulation of the RSV CP, compared with that in WT plants (Figure 6F). We did not observe statistical differences in *L. striatellus* survival on OE-OsMEL, *Osmel*, or OE-SHMT1 compared to WT *O. sativa*.

Punch inoculation of hemibiotrophic fungal pathogen *M. oryzae* (Guy 11) conidia on these transgenic *O. sativa* plants demonstrated that OE-OsMEL *O. sativa* plants were more resistant to *M. oryzae*, with reduced lesion size, whereas *Osmel* and OE-OsSHMT1 *O. sativa* plants were more susceptible (Figure 6, G–J). Spray inoculation confirmed that OE-OsMEL *O. sativa* plants were more resistant and *Osmel O. sativa* plants were more susceptible to *M. oryzae* (Supplemental Figure S22). Following inoculation with hemibiotrophic bacterial leaf blight pathogen *Xoo* (PXO99A), the lesion length was much longer in *Osmel* or OE-OsSHMT1 *O. sativa* and significantly shorter in OE-OsMEL *O. sativa* plants than in the WT control (Figure 6, K–N). Taken together, these results demonstrate that the OsMEL and OsSHMT1 play similar immunity regulating functions as their orthologs in dicots, and the MEL–SHMT1 module is an evolutionarily conserved regulator of plant broad-spectrum resistance.

Discussion

MEL–SHMT1-mediated regulation of plant immunity is associated with both microtubules and mitochondria

A mesh of cytoskeleton stretches from the nucleus to the plasma membrane constructing a complex, dynamic, and high-speed signaling network in cells (Hardham, 2013; Li and Day, 2019). This cytoskeleton works as the frontline of plant defense and pathogen virulence, providing a platform for pathogens–plant contact and battle (Li and Day, 2019). Microtubules, a key component of the cytoskeleton, have been deciphered to be involved in the activation and signaling of plant immunity during the infection by fungal, bacterial, or viral pathogens (Hardham, 2013; Wang et al., 2016; Horníková et al., 2020). As a key player responsible for regulating eukaryotic cellular homeostasis responses, mitochondria supply ATP and biosynthetic intermediates for energy metabolism, redox, and cell death (West et al., 2011; Lisowski et al., 2018). Beyond their primary role as the cellular "energy plant," as a centrally positioned hub in the mammalian and plant innate immune systems, mitochondria are one of the major sources for the generation of intracellular

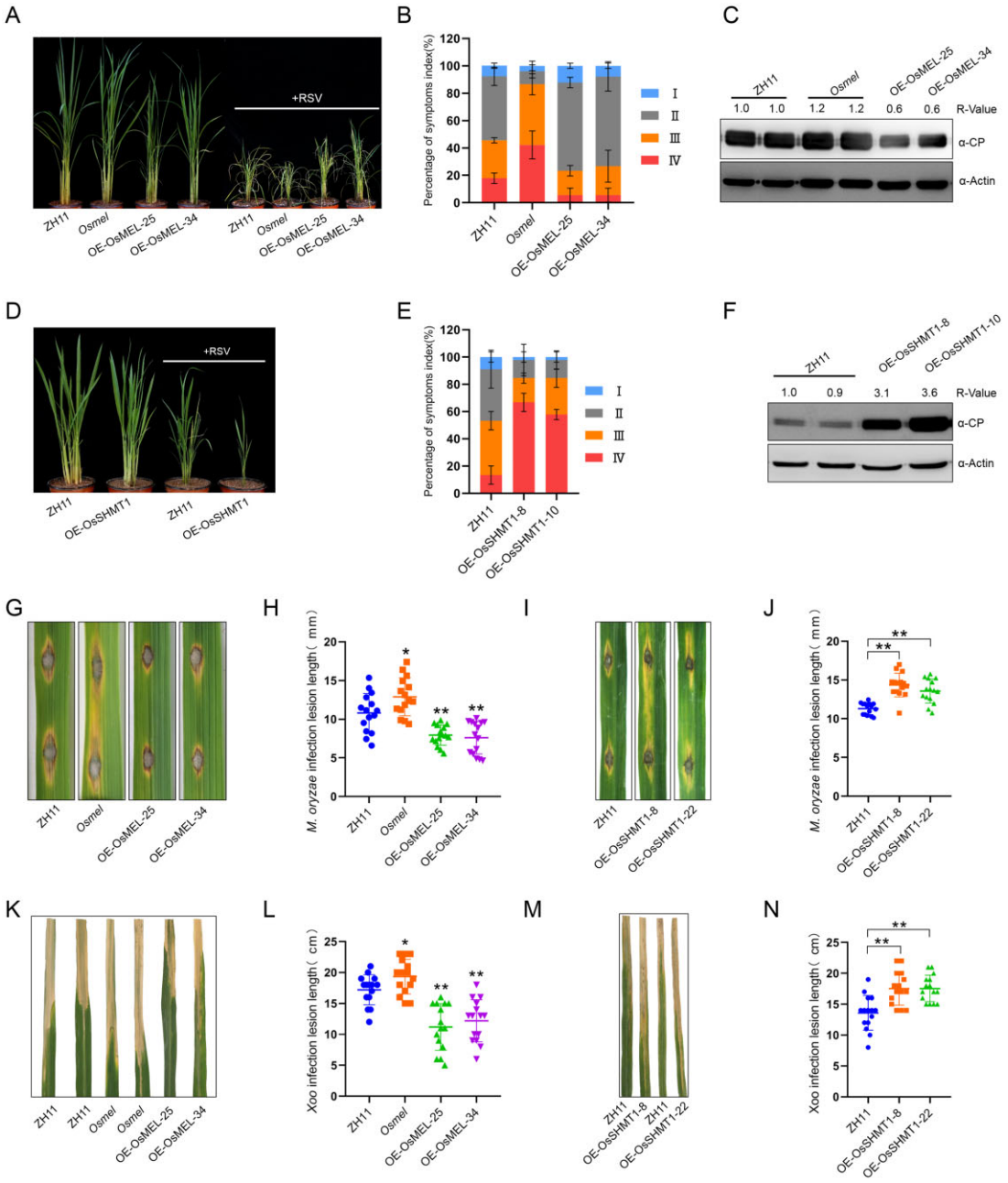

Figure 6 OsMEL–OsSHMT1 module enhances rice broad-spectrum disease resistance. A–C, Comparisons of symptoms (A), symptom severity (B), and CP accumulation (C) in WT (ZH11), *OsMEL* overexpressing transgenic (OE-OsMEL-25/34), *OsMEL* knockout (*Osmel*) *O. sativa* (Cultivar ZH11) plants after RSV infection. Picture was taken at 40 dpi. Actin was used as a loading control. Data are means ± SD (n = 45). D–F, Comparisons of symptoms (D), symptom severity (E), and CP accumulation (F) in ZH11 or *OsSHMT1*-overexpressing transgenic (OE-OsSHMT1-8/22) *O. sativa* plants after RSV infection. The photograph was taken at 40 dpi. Actin was used as a loading control. Data are means ± SD (n = 45). G and H, Comparisons of symptoms (G) and lesion length (H) in OE-OsMEL-25/34, *Osmel*, and ZH11 *O. sativa* plants after punch inoculation with *M. oryzae*. Lesions were photographed at 5 dpi. Data are means ± SD (n = 15). I and J, Comparisons of symptoms (I) and lesion length (J) in OE-OsSHMT1-8/22 and ZH11 *O. sativa* plants after punch inoculation with *M. oryzae*. Lesions were photographed at 5 dpi. Data are means ± SD (n = 15). K and L, Comparisons of symptoms (K) and lesion length (L) in OE-OsMEL-25/34, *Osmel*, and ZH11 *O. sativa* plants inoculated with *Xoo*. Lesions were photographed at 20 dpi. Data are means ± SD (n = 15). M and N, Comparisons of symptoms (M) and lesion length (N) in OE-OsSHMT1-8/22 and ZH11 *O. sativa* plants inoculated with *Xoo*. Lesions were photographed at 20 dpi. Data are means ± SD (n = 15). All the experiments were performed 3 times with similar results. Asterisks in (H), (J), (L), and (N) mark significant differences according to two-tailed Student's t test; $^{*}P < 0.05$; $^{**}P < 0.01$. In (C) and (F), the bands in the immunoblots were quantified and the relative intensities (R-value) are shown above the band.

ROS (West et al., 2011; Dan Dunn et al., 2015; Li et al., 2017). Mitochondria are dynamic organelles. Precise mitochondrial positioning is essential for many cell types (mammals, yeast, etc.) in response to changes in environment conditions such as biotic or abiotic stress. The intracellular transport of mitochondria mainly relies on the cytoskeleton including microtubule (De Rossi et al., 2018; Melkov and Abdu, 2018). The interaction of mitochondria with some cytoskeletal proteins was found to be involved in the coordination of mitochondrial function (Rostovtseva et al., 2012; Kuznetsov et al., 2020). In our study, we found that the *NbMEL* promoter was activated in response to pathogen invasion (Supplemental Figures S2 and S4), and the activated microtubule-localized MEL interacts with mitochondrion-localized SHMT1 (Figure 3; Supplemental Figure S6). The interaction between MEL and SHMT1 leads to SHMT1-dependent mtROS generation, activation of MAPK cascades, and reprogramming of defense-related transcripts, ultimately leading to attenuated viral, fungal, and bacterial invasion (Figure 2), indicating that the MEL-SHMT1-mediated regulation of plant immunity may closely be associated with both microtubules and mitochondria.

MEL targets SHMT1 for 26S proteasome degradation

We demonstrate that the MEL–SHMT1 module can regulate plant immunity. The broad-spectrum resistance of *MEL*-overexpressing plants is likely dependent on MEL interacting with, ubiquitinating, and targeting SHMT1 for 26S proteasome degradation (Figures 3 and 4). Interestingly, we showed that endogenous SHMT1 was decreased in plants after infection with various pathogens, including RSV, *M. oryzae*, *B. cinerea*, and *Xoo* (Figure 4; Supplemental Figures S9 and S21). However, NbSHMT1 is relatively stable after flg22 or chitin treatment (Supplemental Figure S23). It seems that depletion of endogenous SHMT1 is a common phenomenon in plant response to pathogen infection. As a critical enzyme in one-carbon metabolism, SHMT reversibly transfers a methyl group from seine to THF, producing glycine and methylene-THF, which provides one-carbon units for nucleotide synthesis, aa homeostasis (glycine, serine, and methionine), methylation, and redox defense (Ducker and Rabinowitz, 2017). Mutation or downregulation of *SHMT1* might interfere with plant one-carbon metabolism, which has been reported to result in folate deficiency that leads to starvation of plant–parasitic nematode (Liu et al., 2012a; Kandoth et al., 2017; Korasick et al., 2020). The fungal pathogens *M. oryzae* and *B. cinerea*, as well as the bacterial pathogen *Xoo*, obtain nutrients from living cells or damaged tissues (Zhang et al., 2018). The aa homeostasis disturbance caused by *MEL* overexpression or *SHMT1* knockout might affect nutrient uptake from host cells by pathogens, negatively influencing pathogen multiplication.

The role of mtROS in plant innate immunity

ROS have been proposed to act as antimicrobial directly or to function as local and systemic signal molecules that trigger antimicrobial defenses (Van Acker and Coenye, 2017; Waszczak et al., 2018). The production of a ROS burst is a ubiquitous response of plants to pathogen invasion and plays a vital role in plant defense against RSV, *M. oryzae*, *B. cinerea*, and *Xoo*. Higher basal ROS accumulation generated from L-ascorbate oxidase has been shown to enhance anti-RSV defense (Wu et al., 2017). Increasing accumulation of ROS in OsBAG4, *ebr1*, and *Oscul3a O. sativa* plants display broad-spectrum resistance to *M. oryzae* and *Xoo* (You et al., 2016; Liu et al., 2017). The *pub25 pub26* double mutant exhibited increased ROS burst and resistance to both *B. cinerea* and *Pto* DC3000 *hrcC*⁻ (Wang et al., 2018). In our study, we found that *MEL* overexpression constitutively generated more ROS that may initiate a plethora of downstream signaling events. Importantly, we found the burst of ROS accumulation from mitochondria in *NbMEL* overexpression and *Nbshmt1* knockout *N. benthamiana* plants, as confirmed by CM-DCFDA staining (Figure 4, I and J). A growing body of evidence has highlighted the vital roles of mtROS in innate immune responses in mammals (Ye et al., 2014; Ducker and Rabinowitz, 2017), but the function of mtROS in plant immune response is still unclear. Our study provides insights into the positive role of mtROS in the regulation of plant innate immunity. Further research will elucidate the downstream signaling events that occurred after mtROS burst.

The potential role of MEL in MAPK cascades

MAPK cascades, consisting of MAPKKK–MAPKK–MAPK, represent a "core signaling module" that links different receptors to their downstream targets and are present in all eukaryotes (Meng and Zhang, 2013). We demonstrated that MEL has high similarity to the N-terminal region of human ZSWIM2 and MEKK1. Both human ZSWIM2 and MEKK1 act as an E3 ligase harboring a SWIM domain and a C4HC3-type RING domain in their N-terminal region, while MEKK1 has an additional protein kinase domain in its C-terminal region (Lu et al., 2002; Nishito et al., 2006). The C-terminal kinase domain of human MEKK1 functions as an activator of extracellular signal-regulated kinases (ERKs), and the N-terminal regulatory region of human MEKK1 negatively regulates ERK1 and ERK2 activation and offers binding sites to a variety of proteins including ERK2, 14-3-3, α-actin, and c-Jun amino-terminal kinases (JNKs) (Karandikar et al., 2000; Bonvin et al., 2002; Lu et al., 2002; Rieger et al., 2012). In plants, overexpression of plant MEKK1 (homologous to human MEKK1 kinase domain) leads to constitutive MAP kinase activation (Yang et al., 2021). We found overexpression of MEL leads to constitutive activation of plant MAP kinases that are closely related to the mammalian ERK subfamily of MAP kinases (Figure 2, C and D; Meng and Zhang, 2013). Thus it will be interesting to know whether MEL can directly interact with plant MAP kinases and decipher the molecular mechanism of how the N-terminal region of human MEKK1 inhibits ERK1 and ERK2 while plant MEL activates plant MAP kinases. Expression of human ZSWIM2 or MEKK1 efficiently promotes apoptosis (Bonvin et al., 2002; Lu et al., 2002; Nishito et al., 2006). Transient overexpression of *MEL*

induced HR-like cell death, which shares morphological and mechanistic features with mammalian apoptosis (Figure 2, A and B; Lord and Gunawardena, 2012). Notably, similarly to *MEL* transient overexpression, transient overexpression of some plant MAPKKK genes such as *AtMEKK2* (Kong et al., 2012), *MAPKKK5* (Yamada et al., 2016), *MAPKKKα* (del Pozo et al., 2004), and *MAPKKKε* (King et al., 2014) also leads to over-accumulation of H_2O_2 and pathogen-independent activation of cell death. Although plants possess dozens of MAPKKKs, none of them have been described to date as having an N-terminal regulatory region containing SWIM and C4HC3-type RING domains (Hamel et al., 2006). It seems that plants evolved a unique MEL protein containing SWIM and C4HC3-type RING domains that is different from the mammalian MEL integrated with a protein kinase domain to be a MAPKKK (MEKK1). Further research will be required to untangle the intertwined MAPK cascades signaling webs mediated by MEL in plants.

The YφNL motif in MEL C-terminal region confers specificity of binding to its substrate SHMT1

In the ubiquitination/26S proteasome pathway, substrate specificity is dependent on E3 Ub ligases (Verchot, 2016; Calil and Fontes, 2017). Most canonical RING E3 ligases have their E2-binding domain and the substrate-binding domain together in the RING domain (Deshaies and Joazeiro, 2009). However, we showed that, in MEL, the C4HC3-type RING domain is only responsible for the interaction with the E2. This discrepancy might be due to the different configurations of cysteine and histidine residues in RING domains (Stone et al., 2005; Sun et al., 2019). Intrinsically disordered sequences are highly flexible, and that property enables them to function as hubs in protein-interaction networks (Wright and Dyson, 2015). We showed that MEL utilizes an intrinsically disordered region at its C-terminus to bind SHMT1 (Figure 5, A and B). Intrinsically disordered regions function in substrate recognition in the yeast proteins San1, Bag6, and some human E3 ligases (Rosenbaum et al., 2011; Wang et al., 2011; Boomsma et al., 2016). The physical characteristics of intrinsically disordered regions, such as the presence of small recognition elements and conserved sequence motifs to mediate binding interactions, allow an exquisite level of control of cellular signaling processes (Wright and Dyson, 2015); this notion is further supported by our finding that the evolutionarily conserved YφNL motif, embedded in MEL C-terminal intrinsically disordered region, confers the ability to bind its substrate SHMT1 with high specificity (Figure 5).

MEL recognizes and ubiquitinates its substrates in a homodimeric form

Dimerization is a common theme for proteins involved in immune processes, including the activation of many mammalian and plant pattern recognition receptors (Liu et al., 2012b; Hayafune et al., 2014). RING E3 ligases have also been found to form homodimers or heterodimers dependent on the RING domain or other domains outside (Deshaies and Joazeiro, 2009; Metzger et al., 2014). The SWIM domain has been reported to be an ancient metal-binding module, involved in DNA binding and protein–protein interactions (Makarova et al., 2002). In our research, we reveal that MEL converts from monomer to homodimer in response to pathogen infection, and homodimer formation is dependent on its N-terminal SWIM domain (Figure 5, F–J). Mutations in the C4HC3-type RING domain or the YφNL motif do not affect MEL homodimerization. However, mutating Cys-70, Cys-72, and Cys-79 of SWIM domain to Ala causes MEL conversion to a monomer, which does not affect MEL self-ubiquitination, but remarkably impairs MEL self-interaction, and abolishes MEL interacting with and ubiquitinating on SHMT1, suggesting that MEL recognizes and ubiquitinates its substrates in a homodimeric form (Figures 1, D, 3, C, and 5, F). We further showed that DTT disrupts MEL homodimerization, indicating that MEL homodimerization via intermolecular disulfide bonds (Figure 5H). Oxidation of protein cysteine thiols to disulfides represents molecular switches for transferring oxidant signals into dynamic biological responses (Waszczak et al., 2018; Wu et al., 2020). The three-cysteine aa in the SWIM domain were shown to act as sites for oxidation sensing, indicating that MEL conversion between monomer and homodimer is redox dependent. However, the molecular mechanism underlying how Cys in the MEL SWIM domain is oxidized to form intermolecular disulfide bonds-dependent homodimerization and reduced to prevent constitutive activation remains to be determined.

Overall, we provide evidence showing that infections with multiple pathogens induce *MEL* transcriptional expression, and then the formation of MEL homodimers activates MEL E3 ligase activity, triggering SHMT1 degradation by the 26S proteasome pathway, and causing ROS generation from mitochondria followed by activation of plant immune responses conferring broad-spectrum resistance to pathogen invading (Figure 7). Our study provides a fundamental conceptual framework for the future engineering of the MEL–SHMT1 module to fine-tune plant immune responses and to confer staple crops with broad-spectrum resistance to multiple pathogens.

Materials and methods

Plant materials, plant transformation, and agroinfiltration

The full-length ORFs of *NbMEL*, *NbSHMT1*, *OsMEL*, and *OsSHMT1* were amplified from *N. benthamiana* or *O. sativa* cDNA generated by reverse transcription of total RNA. cDNA was synthesized using ReverTra Ace qPCR RT Master Mix with gDNA Remover (TOYOBO, Osaka, Japan) according to the manufacturer's instructions. Point mutations were introduced into *NbMEL* or *OsMEL* by site-direct mutagenesis. In our experiment, Phusion High-Fidelity DNA polymerase (New England Biolabs, Ipswich, MA, USA) was used in all primary PCR amplifications. All primers used for cloning in this study are listed in Supplemental Table S1.

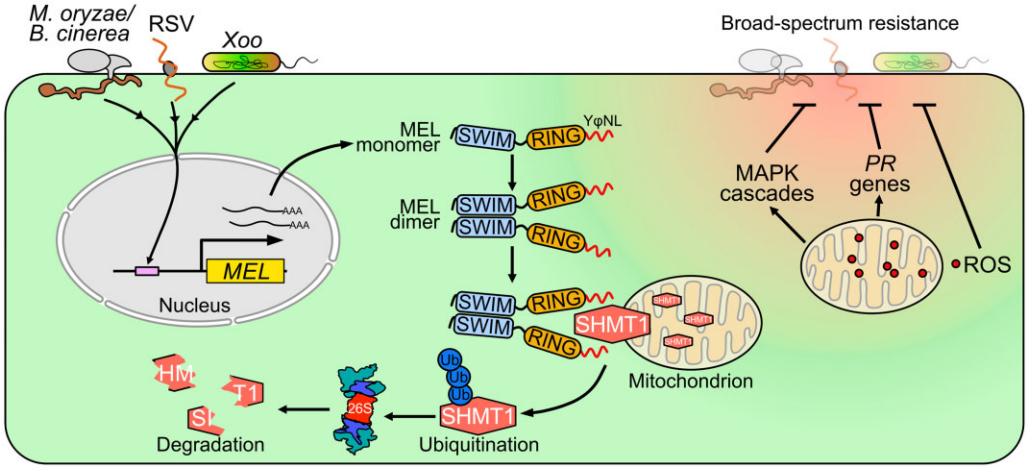

Figure 7 Working model for MEL regulation of plant broad-spectrum resistance against pathogens. Microtubule-localized C4HC3 RING-type E3 ligase (MEL) transcript is activated by the invasion of pathogens. MEL forms homodimers through intermolecular disulfide bonds depending on the SWIM domain and then hijacks its substrate SHMT1 through the YφNL motif, triggering SHMT1 ubiquitination and 26S proteasome-dependent degradation. SHMT1 localize on mitochondria. The degradation of SHMT1 initiates a plant immune signaling cascade, including enhancement of mtROS generation, activation of MAPK cascades, and activation of defense-related genes, ultimately conferring broad-spectrum resistance to multiple pathogen species in both the dicot *N. benthamiana* and the monocot *O. sativa*.

Nicotiana benthamiana plants were grown in the chamber at 26°C and 65% relative humidity under 16/8-h day/night at a photon fluence rate of 200 ± 10 μmol m^{-2} s^{-1} conditions. *Oryza sativa* plants were grown in the chamber at 28°C and 80% relative humidity under 16/8-h day/night at a photon fluence rate of 300 ± 10 μmol m^{-2} s^{-1} conditions. CRISPR/Cas9-based knockout of *NbMEL* and *NbSHMT1* in *N. benthamiana* plants were generated by transformation with the binary vector BGK01 (Biogle, Hangzhou, China) in-fusion with single-guide RNA designed to target the ORFs and their respective alleles simultaneously. CRISPR/Cas9-based knockout of *OsMEL* or *OsSHMT1* in ZH11 (*O. sativa ssp, Japonica*) were generated by transformation with the binary vector BGK03 (Biogle, Hangzhou, China) in-fusion with single-guide RNA designed to target the ORFs. The synthesized sgRNA oligo was annealed and then ligated to BGK01 or BGK03 with T4 DNA ligase (Thermo Fisher, Waltham, MA, USA). All single-guide RNA used for cloning in this study are listed in Supplemental Table S1.

For transgenic overexpression of *NbMEL*, *NbMEL(H179Y)*, *NbMEL(mSWIM)*, and *NbMEL(YφNL)*, *Agrobacterium tumefaciens* EHA105 strains carrying 2 × 35S-NbMEL/NbMEL(H179Y)/NbMEL(mSWIM)/NbMEL(YφNL)-flag were used for transformation in *N. benthamiana* plants using standard protocols (Fu et al., 2018). For overexpression of *OsMEL*, *NbMEL*, and *OsSHMT1* in rice ZH11, *A. tumefaciens* EHA105 carrying 2 × 35S-OsMEL/NbMEL/OsSHMT1-flag were used for transformation using standard protocols (Fu et al., 2018). RT-qPCR and immunoblot were conducted to verify the gene expression. Primers are listed in Supplemental Table S1.

Five/seven-leaf *N. benthamiana* plants were used for *Agrobacterium* infiltration, as described before (Hu et al., 2020). Briefly, the transformed *A. tumefaciens* (EHA105) were grown individually until an OD_{600} of 0.6. The cultures were collected and resuspended in inoculation buffer (10-mM $MgCl_2$, 100-mM MES (pH 5.7), 2-mM acetosyringone) at room temperature. The suspensions were adjusted to an OD_{600} of 0.5 and then used for agroinfiltration in five/seven-leaf *N. benthamiana* plants.

RSV, *M. oryzae*, *X. oryzae* pv. *oryzae*, and *B. cinerea* inoculation

Crude extracts from RSV-infected *O. sativa* leaves ground in phosphate buffer (0.1 M) were used for rub-inoculation in five/seven-leaf *N. benthamiana* plants. After 12-h incubation in the dark, plants were transferred to the growth chamber. RSV CP accumulation was evaluated by immunoblotting with an anti-CP antibody (Huang et al., 2019). For RSV inoculation in *O. sativa*, RSV-viruliferous *L. striatellus* was transferred onto four-leaf stage rice seedlings for 72 h and then removed. Fifteen to 20 plants were used for each treatment and RSV-inoculated seedlings were transferred back to insect-free chamber to observe symptom development daily.

Magnaporthe oryzae isolate Guy11 was used for inoculation. *Magnaporthe oryzae* was grown in a growth chamber at 25°C in the 12-h/12-h day/night conditions. *Magnaporthe oryzae* spores were collected in sterile water, and the spore concentration in the suspension was adjusted to 1×10^5 conidia/mL and used for punch or spray inoculation. For punch inoculation, dip 5-μL spore suspension for each drop at two spots on each leaf, kept in moist conditions in a culture dish, then transferred to the growth chamber at 25°C and 90% relative humidity. Lesion length was measured at 5 dpi. For spray-inoculation, conidial suspensions with 1×10^5 conidia/milliliter diluted in 0.05% Tween-20 were spray-inoculated using an artist's airbrush onto rice plants. Inoculated seedlings were kept in black plastic bags

for 24 h to maintain high humidity and then transferred to a growth chamber at 25°C and 90% relative humidity. Relative fungal DNA was calculated by RT-qPCR detecting *M. oryzae* Pot2 DNA against the rice genomic Ub DNA (Park et al., 2012). All inoculation experiments were repeated 3 times independently.

Rice plants were inoculated with *Xoo* by the leaf-clipping method. Bacterial cells from the *Xoo* strain PXO99A were suspended in distilled water and adjusted to 1×10^8 cfu/mL. Scissors were dipped into the bacterial suspensions and then used to remove the distal tips (3 cm) of flag leaves. At least five individual plants and three tillers of each plant were inoculated *Xoo*. The infected plants were grown in a growth chamber at 28°C in a 12/12-h day/night regime. The disease was scored by measuring the lesion length at 20 dpi.

Potato dextrose agar medium (200-g/L potato, 20-g/L glucose, 15-g/L agar) was used for *B. cinerea* strain B05.10 cultivation. Plates were incubated at 24°C with a 12/12-h day/night regime. Conidia were collected and washed twice by centrifugation (8,000 *g*, 5 min) before being resuspended in potato dextrose broth. A single droplet of 5-μL spore suspension (5×10^6 spores/mL) was placed on a leaf of five/seven-leaf plants. Inoculated plants were kept under a transparent dome to maintain high humidity until disease lesions were recorded 4 days later.

Histochemical staining of GUS, H_2O_2, and cell death

For GUS staining, plant tissues and leaves were carefully transferred to 50-mL polypropylene tubes and completely covered with GUS staining solution (50-mM sodium phosphate pH 7.0, 10-mM EDTA, and 0.5-mg/mL X-gluc). Tubes were incubated at 37°C in the dark overnight. The GUS staining solution was discarded, and absolute ethanol was added, samples were incubated in the water bath at 90°C to clear the chlorophyll. H_2O_2 staining was performed as described previously with minor modification (Bach-Pages and Preston, 2018). Briefly, leaves were carefully transferred to 50-mL polypropylene tubes and completely covered with freshly prepared DAB solution (1-mg/mL, PH 3.8; Sigma, St Louis, MO, USA) and then kept in the dark for 6–8 h. The DAB solution was discarded, absolute ethanol was added, and the tubes were incubated in the water bath at 90°C to clear the chlorophyll. Cell death staining by trypan blue was performed as described previously (Bach-Pages and Preston, 2018).

H_2O_2 measurement

H_2O_2 was measured using the Amplex Red Hydrogen Peroxide/Peroxidase Assay kit (Invitrogen, Waltham, MA, USA). Briefly, three 100 mg independent pieces of leaf discs from each treatment were pooled and ground to a fine powder with liquid nitrogen, then 500-μL 50-mM sodium phosphate (pH 7.4) was added to the power as one replicate, the mixture was incubated on ice for 10 min. After centrifuging at 12,000 *g* for 10 min at 4°C, the supernatant was used for measuring H_2O_2 by the Amplex Red Hydrogen Peroxide/Peroxidase Assay Kit (Invitrogen) following the manufacturer's directions. The fluorescence was measured with a fluorescence microplate reader (Molecular Devices, FlexStation3) using excitation at 530 nm and fluorescence detection at 580–600 nm. The fluorescence value in control was set as 1. Measurements were conducted at least 3 times.

Confocal microscopy observation of cellular ROS by DCFDA

Membrane-permeable ROS indicator chloromethyl-2′,7′-dichlorodihydrofluorescein diacetate (CM-H2DCFDA) was used for intracellular ROS measurement as described previously with some modifications (Shang-Guan et al., 2018). Five/seven-leaf *N. benthamiana* plants were preinfiltrated with COX4-mCherry, 48-h postinfiltration, the infiltrated leaves stain with CM-H2DCFDA for 30 min in the dark followed by washing with distilled water. DCF fluorescence was observed by confocal microscope (Zeiss 880) with excitation/emission spectra at 495/529 nm. COX4-mCherry was observed by confocal microscope with excitation/emission spectra at 580/610 nm.

Y2H assays

Yeast (Y2HGold) competent cells were chemically induced with 100 mM LiAc for 30 min at 30°C. Competent cells were resuspended in suspension solution (30% PEG3350, 100 mM LiAc, 250-ng/mL Salmon DNA). Five hundred nanogram of each plasmid were mixed with 350-μL competent cells, then subjected to heat shock at 42°C for 30 min. Then the competent cell mix was centrifuged at 16,000 *g* at room temperature for 1 min and resuspended in 50-μL H_2O. Co-transformants were grown in SC/−Leu−Trp for 3 days at 30°C and then cultured on a selection medium (SC/−Leu−Trp−His or SC/−Leu−Trp−His−Ade) to detect the interactions.

Co-IP assays

Agrobacterium tumefaciens EHA105 strains carrying the expression constructs were infiltrated into *N. benthamiana* leaves. Total proteins were extracted with IP buffer containing 50-mM TRIS-MES pH 8.0, 0.5 M sucrose, 1-mM $MgCl_2$, 10-mM EDTA, 5-mM DTT, 50-μM MG132, and proteinase inhibitor cocktail (Roche, Basel, Switzerland) followed by centrifugation at 12,000 *g* at 4°C for 20 min. Then the soluble proteins were immunoprecipitated with 30-μL anti-Flag magnetic beads (Sigma) at 4°C for 2 h with slow shaking. Beads were washed 3 times using IP buffer. Then, the bound protein was eluted by incubating with 50 μL of 20-μg/mL 3 × Flag peptide (Sigma) for 1 h. The eluted protein was separated by sodium dodecyl sulfate polyacrylamide gel electrophoresis (SDS-PAGE) and detected by immunoblotting.

In vitro ubiquitination assays

In vitro ubiquitination assay was performed as described previously (Shen et al., 2016). GST-fused, His-fused, and MBP-fused recombinant proteins were expressed in *Escherichia coli* strain BL21 and affinity-purified with GST-

binding, His-binding, and MBP-binding resin, respectively. Purified GST-tagged NbMEL was incubated with His-E1(AtUBA1), Human E2 (UB2D2/UBCH5b), and HA-Ub at 30°C within ubiquitination buffer (50-mM Tris–HCl pH 7.4, 2-mM ATP, 5-mM $MgCl_2$, and 2-mM DTT) followed by agitation for 1.5 h. After the reaction, SDS loading buffer was added to the samples, and the samples were heated to 95°C for 10 min, followed by immunoblotting. E1 was obtained from the Yan Liang laboratory (Zhejiang University). Human E2 (UB2D2) was obtained from Qi Xie's laboratory (Chinese Academy of Science). To determine whether NbSHMT1/OsSHMT1 protein could be ubiqutinated by NbMEL/OsMEL, purified MBP-tagged NbSHMT1/OsSHMT1 was incubated at 30°C with the ubiquitination mixture for 1.5 h. SDS loading buffer was added to the samples and the samples were heated to 95°C for 10 min, followed by immunoblotting.

In vivo ubiquitination assays

To detect ubiquitination of SHMT1 in vivo, we transiently co-expressed NbSHMT1-Flag, NbMEL-Myc, and Ub-Myc in *N. benthamiana* leaves, 100-μM MG132 was preinfiltrated into infiltrated leaves 4 h before total protein extraction. Total proteins were extracted using IP buffer and NbSHMT1-Flag was immunoprecipitated using anti-Flag beads. The poly-ubiquitination of NbSHMT1-Flag was detected with the anti-Flag or anti-Ub antibody.

BiFC and subcellular localization assays

BiFC and subcellular localization assays were performed as described previously (Fu et al., 2018). To test the microtubule localization of NbMEL or OsMEL, 50-mM microtubule-depolymerizing drug oryzalin was used. *Agrobacterium tumefaciens* EHA105 strains carrying constructs to express NbMEL-GFP or OsMEL and MAP65-mCherry were co-infiltrated into the abaxial side of *N. benthamiana* leaves. After being expressed for 24 h, the leaf was re-infiltrated with DMSO or 50 mM oryzalin. About 12 h later of infiltration, samples were observed under the confocal microscope (Zeiss 880). The MitoProtII program was used for predicting NbSHMT1 mitochondrial targeting sequences (https://ihg.gsf.de/ihg/mitoprot.html). To stain mitochondria by Mito-Tracker Red CMXRos (Beyotime, Jiangsu, China), 1-mM Mito-Tracker Red CMXRos was infiltrated into *N. benthamiana* leaves that had transiently expressed NbSHMT1-GFP, after incubation for 30 min, samples were observed under the confocal microscope (Zeiss 880) with excitation/emission spectra at 579/599 nm. Gold labeling was visualized using an H7650 TEM (Hitachi, Ibaraki, Japan) at an acceleration voltage of 80 kV.

Chemical treatments and semi-in vivo protein degradation assay

Semi-in vivo and in vivo protein degradation analyses were performed as described previously (Shen et al., 2016). Briefly, the chemical concentration is 20-mM ATP (Sigma) dissolved in ddH_2O, and 100-μM MG132 (Sigma) or cycloheximide (Sigma) dissolved in DMSO. Samples were extracted with native extraction buffer (50-mM Tris-MES pH 8.0, 0.5 M sucrose, 1-mM $MgCl_2$, 10-mM EDTA, 5-mM DTT, proteinase inhibitor cocktail [Roche]). For in vitro oligomerization assay, total protein was extracted from *N. benthamiana* leaves by native extraction buffer without DTT. The supernatant of total protein extracts was treated with 0–100 mM DTT at 25°C for 20 min, followed by adding SDS loading buffer and the samples were heated to 95°C for 10 min. The samples were then separated on 12% nonreducing (-DTT) SDS–PAGE followed by immunoblotting.

Data mining and phylogenetic analyses

MEL homologous proteins in the plant kingdom were retrieved by Blast search in EnsemblPlants (http://plants.ensembl.org/index.html). All retrieved MEL orthologs were submitted to InterProScan (http://www.ebi.ac.uk/InterProScan/) to confirm the presence of SWIM (IPR006564) and C4HC3-type RING (IPR013083) domains. To investigate the evolutionary relationship of plant MEL orthologs, the MEL sequence from 17 dicots (*Actinidia chinensis*, *Arabidopsis thaliana*, *Beta vulgaris*, *Corchorus capsularis*, *Cucumis sativus*, *Daucus carota*, *Gossypium raimondii*, *Helianthus annuus*, *Manihot esculenta*, *Medicago truncatula*, *Nicotiana attenuata*, *Populus trichocarpa*, *Prunus persica*, *Solanum lycopersicum*, *Solanum tuberosum*, *Theobroma cacao*, *Vitis vinifera*), seven monocots (*Brachypodium distachyon*, *Leersia perrieri*, *Musa acuminate*, *O. sativa*, *Panicum hallii*, *Triticum aestivum*, *Zea mays*), four algae and ferns (*Amborella trichopoda*, *Chlamydomonas reinhardtii*, *Physcomitrella patens* and *Selaginella moellendorffii*) were subjected to multiple full-length protein sequence alignment followed by maximum likelihood (ML) phylogenetic tree construction using MEGA version 7 software (Kumar et al., 2016).

Immunoblotting and antibodies

Immunoblotting was performed as described previously (Fu et al., 2018). Membranes were probed with primary anti-Flag (Sigma-Aldrich, St Louis, MO, USA; Cat#: M8823); anti-MYC (Vazyme, Nanjing, China; Cat#: Ab307-02); anti-GFP (Abclonal, Woburn, MA, USA; Cat#: AE012) anti-Actin (ABclonal, Cat#: AC009); anti-SHMT1 (Agrisera, Vännäs, Sweden; Cat#: AS05 075); anti-MBP (ABclonal, Cat#: AE016); anti-His (Vazyme; Cat#: Ab305-02); anti-Ub (Agrisera; Cat#: AS08 307A); anti-p44/42 MAPK (Erk1/2) (Cell Signaling Technology, Danvers, MA, USA; Cat#:9101S); anti-HA (Roche; Cat#:11583816001), followed by the corresponding secondary antibodies conjugated to horseradish peroxidase [Goat anti-Rabbit IgG (H + L) Secondary Antibody, HRP (Thermo Fisher; Cat#:31460); Goat anti-Mouse IgG (H + L) Secondary Antibody, HRP (Thermo Fisher; Cat#:31430)]. The mouse monoclonal antibody against the RSV capsid protein was generated in the author's laboratory (Huang et al., 2019). The blotted signal was visualized using chemiluminescence according to the manufacturer's manual (GE Healthcare, Chicago, IL, USA), and signal band quantification was performed with ImageJ (https://imagej.nih.gov/ij/).

Quantification and statistical analysis

All experiments involving measurements, quantifications, and imaging were repeated at least 3 times with similar results. GraphPad Prism version 8 or Excel was used for data plotting and statistical tests. Statistical parameters such as mean ± standard deviation (SD), standard error (SE), or 95% confidence intervals are indicated in figure legends. In all graphs, asterisks mark statistical significance (*$0.01 < P < 0.05$; **$P < 0.01$; NS, $P > 0.05$, not significant) according to two-tailed Student's *t* test (two-tailed).

Accession numbers

Sequence data from this article can be found in the EMBL/GenBank data libraries under accession numbers: NbMEL (MW674931), OsMEL(MW674932), AtMEL (AT5G11620), NbSHMT1-1 (OK377067), NbSHMT1-2 (OK377068), NbSHMT2 (OK377069), NbSHMT3 (OK377070), NbSHMT4 (OK377071), OsSHMT1 (LOC_Os03g52840.1), ZSWIM2 (151112), and MEKK1 (4214).

Supplemental data

The following materials are available in the online version of this article.

Supplemental Figure S1. NbMEL is a C4HC3 RING-type E3 ligase activated by RSV infection and negatively regulates RSV infection (supports Figure 1).

Supplemental Figure S2. Transcript expression and promoter activity assay of *NbMEL* in different *N. benthamiana* plant tissues (supports Figure 1).

Supplemental Figure S3. Analysis of transcript, protein, and growth phenotype of transgenic *N. benthamiana* plants overexpressing *NbMEL* or its mutants (supports Figures 1 and 2).

Supplemental Figure S4. Analysis of *NbMEL* promoter or transcript in response to *B. cinerea* infection or MD (supports Figure 2).

Supplemental Figure S5. Sequence comparison and phylogenetic tree of SHMT homologs from *N. benthamiana*, *O. sativa*, and Arabidopsis (supports Figure 3).

Supplemental Figure S6. NbMEL interacts with NbSHMT1 (supports Figure 3).

Supplemental Figure S7. NbSHMT1 is ubiquitinated by NbMEL (supports Figure 3).

Supplemental Figure S8. Specificity of SHMT1 antibody (supports Figures 3 and 4).

Supplemental Figure S9. NbSHMT1 protein downregulated in response to RSV infection quantified by iTRAQ (supports Figure 4).

Supplemental Figure S10. Relative mRNA levels of *NbSHMT1* in response to RSV or *B. cinerea* infection (supports Figure 4).

Supplemental Figure S11. *NbSHMT1* knock-out and overexpression in *N. benthamiana* (supports Figure 4).

Supplemental Figure S12. NbSHMT1 localizes in mitochondria (supports Figure 4).

Supplemental Figure S13. VDAC1 accumulation in OE-NbMEL and *Nbshmt1 N. benthamiana* plant leaves (supports Figure 4).

Supplemental Figure S14. BiFC assay to test the self-interaction of NbMEL or its mutants, and the interaction between NbMEL mutants and NbSHMT1 (supports Figure 5).

Supplemental Figure S15. Analysis of transcript, protein expression of transgenic *N. benthamiana* plants overexpressing *NbMEL(mYφNL)* or *NbMEL(mSWIM)* (supports Figure 5).

Supplemental Figure S16. MEL is highly conserved in the plant kingdom (supports Figure 5, Figure 6).

Supplemental Figure S17. Subcellular localization of OsMEL and OsSHMT1 (supports Figure 6).

Supplemental Figure S18. OsMEL is an E3 ligase that interacts, ubiquitinates, and promotes degradation of OsSHMT1 (supports Figure 6).

Supplemental Figure S19. The phenotype of *OsMEL* overexpression (OE-OsMEL-25/34) and knockout (*Osmel*) *Oryzae sativa* plants (supports Figure 6).

Supplemental Figure S20. The phenotype of OsSHMT1 overexpression (OE-OsSHMT-8/22) and knockout (*Osshmt1*) *O. sativa* plants (supports Figure 6).

Supplemental Figure S21. Comparison of endogenous OsSHMT1 accumulation in RSV (A), *M. oryzae* (B), or *Xoo* (C)-infected *O. sativa* plants with mock (CK-) *O. sativa* plants (supports Figure 6).

Supplemental Figure S22. OsMEL positively regulates *O. sativa* plants resistance to *M. oryzae* (supports Figure 6).

Supplemental Figure S23. NbSHMT1 protein accumulation assay under flg22 or chitin treatment (supports Figure 4).

Supplemental Table S1. Primers used in this work.

Acknowledgments

We thank Dr Rosa Lozano-Duran (Shanghai Center for Plant Stress Biology, Chinese Academy of Sciences) for revising and critical comments on the manuscript; Dr Qi Xie (Institute of Genetics and Developmental Biology, Chinese Academy of Sciences) for help in in vitro ubiquitination assays; Dr Zhengyi Wang for offering fungal pathogen *M. oryzae* (Guy 11) (Zhejiang University) and Dr Bin Li (Zhejiang University) for offering bacterial leaf blight pathogen *Xoo* (PXO99A); Dr Yongbo Hong (China National Rice Research Institute) for help in *Xoo* inoculation. Dr Yijun Zhou and Dr Tong Zhou (Institute of Plant Protection, Jiangsu Academy of Agricultural Sciences) for assistance in RSV inoculation; Dr Huanbin Zhou (Institute of Plant Protection, Chinese Academy of Agricultural Sciences) for help in rice transformation. Dr Li Xie (Zhejiang University) for help in immunegold labeling transmission electron microscopy analysis. Dr Zhenyu Qi (Agricultural Experiment Station, Zhejiang University) for help in the rice greenhouse culture.

Funding

This work was supported by grants from the National Natural Science Foundation of China for Youth Scholars (31801701), National Natural Science Foundation of China (31772125), and the Earmarked Fund for Modern Agro-industry Technology Research System (nycytx-001).

Conflict of interest statement. The authors declare that they have no conflict of interest.

References

Bach-Pages M, Preston GM (2018) Methods to quantify biotic-induced stress in plants. Methods Mol Biol **1734**: 241–255

Birkenbihl RP, Liu S, Somssich IE (2017) Transcriptional events defining plant immune responses. Curr Opin Plant Biol **38**: 1–9

Bonvin C, Guillon A, van Bemmelen MX, Gerwins P, Johnson GL, Widmann C (2002) Role of the amino-terminal domains of MEKKs in the activation of NF kappa B and MAPK pathways and in the regulation of cell proliferation and apoptosis. Cell Signal **14**: 123–131

Boomsma W, Nielsen SV, Lindorff-Larsen K, Hartmann-Petersen R, Ellgaard L (2016) Bioinformatics analysis identifies several intrinsically disordered human E3 ubiquitin-protein ligases. PeerJ **4**: e1725

Boutrot F, Zipfel C (2017) Function, discovery, and exploitation of plant pattern recognition receptors for broad-spectrum disease resistance. Ann Rev Phytopathol **55**: 257–286

Calil IP, Fontes EPB (2017) Plant immunity against viruses: antiviral immune receptors in focus. Ann Bot **119**: 711–723

Cubillos-Rojas M, Schneider T, Sánchez-Tena S, Bartrons R, Ventura F, Rosa JL (2016) Tris-acetate polyacrylamide gradient gel electrophoresis for the analysis of protein oligomerization. Anal Bioanal Chem **408**: 1715–1719

Dan Dunn J, Alvarez LA, Zhang X, Soldati T (2015) Reactive oxygen species and mitochondria: a nexus of cellular homeostasis. Redox Biol **6**: 472–485

De Rossi María C, Levi V, Bruno L (2018) Retraction of rod-like mitochondria during microtubule-dependent transport. Biosci Rep **38**: BSR20180208

del Pozo O, Pedley KF, Martin GB (2004) MAPKKKalpha is a positive regulator of cell death associated with both plant immunity and disease. EMBO J **23**: 3072–3082

Deshaies RJ, Joazeiro CA (2009) RING domain E3 ubiquitin ligases. Ann Rev Biochem **78**: 399–434

Ducker GS, Rabinowitz JD (2017) One-carbon metabolism in health and disease. Cell Metab **25**: 27–42

Fu S, Xu Y, Li C, Li Y, Wu J, Zhou X (2018) Rice stripe virus interferes with S-acylation of remorin and Induces its autophagic degradation to facilitate virus infection. Mol Plant **11**: 269–287

Gupta R, Yang Q, Dogra SK, Wajapeyee N (2017) Serine hydroxymethyl transferase 1 stimulates pro-oncogenic cytokine expression through sialic acid to promote ovarian cancer tumor growth and progression. Oncogene **36**: 4014–4024

Hamel LP, Nicole MC, Sritubtim S, Morency MJ, Ellis M, Ehlting J, Beaudoin N, Barbazuk B, Klessig D, Lee J, et al. (2006) Ancient signals: comparative genomics of plant MAPK and MAPKK gene families. Trend Plant Sci **11**: 192–198

Hardham AR (2013) Microtubules and biotic interactions. Plant J **75**: 278–289

Hayafune M, Berisio R, Marchetti R, Silipo A, Kayama M, Desaki Y, Arima S, Squeglia F, Ruggiero A, Tokuyasu K, et al. (2014) Chitin-induced activation of immune signaling by the rice receptor CEBiP relies on a unique sandwich-type dimerization. Proc Natl Acad Sci USA **111**: E404–E413

Horníková L, Bruštíková K, Forstová J (2020) Microtubules in polyomavirus infection. Viruses **12**: 121

Hu T, Song Y, Wang Y, Zhou X (2020) Functional analysis of a novel βV1 gene identified in a geminivirus betasatellite. Sci China Life Sci **63**: 688–696

Huang DQ, Chen R, Wang YQ, Hong J, Zhou XP, Wu JX (2019) Development of a colloidal gold-based immunochromatographic strip for rapid detection of Rice stripe virus. J Zhejiang Univ Sci B **20**: 343–354

Ismayil A, Yang M, Liu Y (2020) Role of autophagy during plant-virus interactions. Semin Cell Dev Biol **101**: 36–40

Kandoth PK, Liu S, Prenger E, Ludwig A, Lakhssassi N, Heinz R, Zhou Z, Howland A, Gunther J, Eidson S, et al. (2017) Systematic mutagenesis of serine hydroxymethyltransferase reveals an essential role in nematode resistance. Plant Physiol **175**: 1370–1380

Karandikar M, Xu S, Cobb MH (2000) MEKK1 binds raf-1 and the ERK2 cascade components. J Biol Chem **275**: 40120–40127

King SR, McLellan H, Boevink PC, Armstrong MR, Bukharova T, Sukarta O, Win J, Kamoun S, Birch PR, Banfield MJ (2014) Phytophthora infestans RXLR effector PexRD2 interacts with host MAPKKK ε to suppress plant immune signaling. Plant Cell **26**: 1345–1359

Kong Q, Qu N, Gao M, Zhang Z, Ding X, Yang F, Li Y, Dong OX, Chen S, Li X, et al. (2012) The MEKK1-MKK1/MKK2-MPK4 kinase cascade negatively regulates immunity mediated by a mitogen-activated protein kinase kinase kinase in Arabidopsis. Plant Cell **24**: 2225–2236

Korasick DA, Kandoth PK, Tanner JJ, Mitchum MG, Beamer LJ (2020) Impaired folate binding of serine hydroxymethyltransferase 8 from soybean underlies resistance to the soybean cyst nematode. J Biol Chem **295**: 3708–3718

Kumar S, Stecher G, Tamura K (2016) MEGA7: molecular evolutionary genetics analysis version 7.0 for bigger datasets. Mol Biol Evol **33**: 1870–1874

Kuznetsov AV, Javadov S, Grimm M, Margreiter R, Ausserlechner MJ, Hagenbuchner J (2020) Crosstalk between mitochondria and cytoskeleton in cardiac cells. Cells **9**: 222

Li P, Day B (2019) Battlefield cytoskeleton: turning the tide on plant immunity. Mol Plant-Microbe Interact **32**: 25–34

Li W, Chern M, Yin J, Wang J, Chen X (2019) Recent advances in broad-spectrum resistance to the rice blast disease. Curr Opin Plant Biol **50**: 114–120

Li W, Deng Y, Ning Y, He Z, Wang GL (2020) Exploiting broad-spectrum disease resistance in crops: from molecular dissection to breeding. Ann Rev Plant Biol **71**: 575–603

Li Z, Ding B, Zhou X, Wang GL (2017) The rice dynamin-related protein OsDRP1E negatively regulates programmed cell death by controlling the release of cytochrome c from mitochondria. PLoS Pathog **13**: e1006157

Lisowski, P., Kannan, P., Mlody, B., Prigione, A. (2018) Mitochondria and the dynamic control of stem cell homeostasis. EMBO Rep **19**: e45432

Liu Q, Ning Y, Zhang Y, Yu N, Zhao C, Zhan X, Wu W, Chen D, Wei X, Wang GL, et al. (2017) OsCUL3a negatively regulates cell death and immunity by degrading OsNPR1 in rice. Plant Cell **29**: 345–359

Liu S, Kandoth PK, Warren SD, Yeckel G, Heinz R, Alden J, Yang C, Jamai A, El-Mellouki T, Juvale PS, et al. (2012a) A soybean cyst nematode resistance gene points to a new mechanism of plant resistance to pathogens. Nature **492**: 256–260

Liu T, Liu Z, Song C, Hu Y, Han Z, She J, Fan F, Wang J, Jin C, Chang J, et al. (2012b) Chitin-induced dimerization activates a plant immune receptor. Science **336**: 1160–1164

Liu W, Liu J, Triplett L, Leach JE, Wang GL (2014) Novel insights into rice innate immunity against bacterial and fungal pathogens. Ann Rev Phytopathol **52**: 213–241

Lord CE, Gunawardena AH (2012) Programmed cell death in *C. elegans*, mammals and plants. Eur J Cell Biol **91**: 603–613

Lu Z, Xu S, Joazeiro C, Cobb MH, Hunter T (2002) The PHD domain of MEKK1 acts as an E3 ubiquitin ligase and mediates ubiquitination and degradation of ERK1/2. Mol Cell **9**: 945–956

Makarova KS, Aravind L, Koonin EV (2002) SWIM, a novel Zn-chelating domain present in bacteria, archaea and eukaryotes. Trend Biochem Sci **27**: 384–386

Marino D, Froidure S, Canonne J, Khaled SB, Khafif M, Pouzet C, Jauneau A, Roby D, Rivas S (2019) Addendum: Arabidopsis ubiquitin ligase MIEL1 mediates degradation of the transcription factor MYB30 weakening plant defence. Nat Commun **10**: 1475

Melkov A, Abdu U (2018) Regulation of long-distance transport of mitochondria along microtubules. Cell Mol Life Sci **75**: 163–176

Meng X, Zhang S (2013) MAPK cascades in plant disease resistance signaling. Ann Rev Phytopathol **51**: 245–266

Metzger MB, Pruneda JN, Klevit RE, Weissman AM (2014) RING-type E3 ligases: master manipulators of E2 ubiquitin-conjugating enzymes and ubiquitination. Biochim Biophys Acta **1843**: 47–60

Moreno JI, Martín R, Castresana C (2005) Arabidopsis SHMT1, a serine hydroxymethyltransferase that functions in the photorespiratory pathway influences resistance to biotic and abiotic stress. Plant J **41**: 451–463

Muhammad T, Zhang F, Zhang Y, Liang Y (2019) RNA interference: a natural immune system of plants to counteract biotic stressors. Cells **8**: 38

Ning Y, Shi X, Wang R, Fan J, Park CH, Zhang C, Zhang T, Ouyang X, Li S, Wang GL (2015) OsELF3-2, an ortholog of arabidopsis ELF3, interacts with the E3 ligase APIP6 and negatively regulates immunity against *Magnaporthe oryzae* in rice. Mol Plant **8**: 1679–1682

Nishito Y, Hasegawa M, Inohara N, Núñez G (2006) MEX is a testis-specific E3 ubiquitin ligase that promotes death receptor-induced apoptosis. Biochem J **396**: 411–417

Park CH, Chen S, Shirsekar G, Zhou B, Khang CH, Songkumarn P, Afzal AJ, Ning Y, Wang R, Bellizzi M, et al. (2012) The *Magnaporthe oryzae* effector AvrPiz-t targets the RING E3 ubiquitin ligase APIP6 to suppress pathogen-associated molecular pattern-triggered immunity in rice. Plant Cell **24**: 4748–4762

Quilis J, Peñas G, Messeguer J, Brugidou C, San Segundo B (2008) The Arabidopsis AtNPR1 inversely modulates defense responses against fungal, bacterial, or viral pathogens while conferring hypersensitivity to abiotic stresses in transgenic rice. Mol Plant-Microbe Interact **21**: 1215–1231

Rieger MA, Duellman T, Hooper C, Ameka M, Bakowska JC, Cuevas BD (2012) The MEKK1 SWIM domain is a novel substrate receptor for c-Jun ubiquitylation. Biochem J **445**: 431–439

Rosenbaum JC, Fredrickson EK, Oeser ML, Garrett-Engele CM, Locke MN, Richardson LA, Nelson ZW, Hetrick ED, Milac TI, Gottschling DE, et al. (2011) Disorder targets misorder in nuclear quality control degradation: a disordered ubiquitin ligase directly recognizes its misfolded substrates. Mol Cell **41**: 93–106

Rostovtseva TK, Gurnev PA, Chen MY, Bezrukov SM (2012) Membrane lipid composition regulates tubulin interaction with mitochondrial voltage-dependent anion channel. J Biol Chem **287**: 29589–29598

Savary S, Willocquet L, Pethybridge SJ, Esker P, McRoberts N, Nelson A (2019) The global burden of pathogens and pests on major food crops. Nat Ecol Evol **3**: 430–439

Senthil-Kumar M, Mysore KS (2013) Nonhost resistance against bacterial pathogens: retrospectives and prospects. Ann Rev Phytopathol **51**: 407–427

Serrano I, Gu Y, Qi D, Dubiella U, Innes RW (2014) The Arabidopsis EDR1 protein kinase negatively regulates the ATL1 E3 ubiquitin ligase to suppress cell death. Plant Cell **26**: 4532–4546

Shang-Guan K, Wang M, Htwe N, Li P, Li Y, Qi F, Zhang D, Cao M, Kim C, Weng H, et al. (2018) Lipopolysaccharides trigger two successive bursts of reactive oxygen species at distinct cellular locations. Plant Physiol **176**: 2543–2556

Shen Q, Hu T, Bao M, Cao L, Zhang H, Song F, Xie Q, Zhou X (2016) Tobacco RING E3 ligase NtRFP1 mediates ubiquitination and proteasomal degradation of a geminivirus-encoded βC1. Mol Plant **9**: 911–925

Stone SL, Hauksdóttir H, Troy A, Herschleb J, Kraft E, Callis J (2005) Functional analysis of the RING-type ubiquitin ligase family of Arabidopsis. Plant Physiol **137**: 13–30

Sun J, Sun Y, Ahmed RI, Ren A, Xie AM (2019) Research progress on plant RING-finger proteins. Genes **10**: 973

Todisco S, Agrimi G, Castegna A, Palmieri F (2006) Identification of the Mitochondrial NAD + Transporter in Saccharomyces cerevisiae. J Biol Chem **281**: 1524–1531

Van Acker H, Coenye T (2017) The role of reactive oxygen species in antibiotic-mediated killing of bacteria. Trend Microbiol **25**: 456–466

Verchot J (2016) Plant virus infection and the ubiquitin proteasome machinery: arms race along the endoplasmic reticulum. Viruses **8**: 314

Wang J, Grubb LE, Wang J, Liang X, Li L, Gao C, Ma M, Feng F, Li M, Li L, et al. (2018) A regulatory module controlling homeostasis of a plant immune kinase. Mol Cell **69**: 493–504.e6

Wang J, Wang Y, Liu X, Xu Y, Ma Q (2016) Microtubule polymerization functions in hypersensitive response and accumulation of H2O2 in wheat induced by the stripe rust. BioMed Res Int **2016**: 7830768

Wang Q, Liu Y, Soetandyo N, Baek K, Hegde R, Ye Y (2011) A ubiquitin ligase-associated chaperone holdase maintains polypeptides in soluble states for proteasome degradation. Mol Cell **42**: 758–770

Waszczak C, Carmody M, Kangasjärvi J (2018) Reactive oxygen species in plant signaling. Ann Rev Plant Biol **69**: 209–236

West AP, Shadel GS, Ghosh S (2011) Mitochondria in innate immune responses. Nat Rev Immunol **11**: 389–402

Wright PE, Dyson HJ (2015) Intrinsically disordered proteins in cellular signalling and regulation. Nat Rev Mol Cell Biol **16**: 18–29

Wu F, Chi Y, Jiang Z, Xu Y, Xie L, Huang F, Wan D, Ni J, Yuan F, Wu X, et al. (2020) Hydrogen peroxide sensor HPCA1 is an LRR receptor kinase in Arabidopsis. Nature **578**: 577–581

Wu J, Yang R, Yang Z, Yao S, Zhao S, Wang Y, Li P, Song X, Jin L, Zhou T, et al. (2017) ROS accumulation and antiviral defence control by microRNA528 in rice. Nat Plants **3**: 16203

Xin XF, He SY (2013) Pseudomonas syringae pv. tomato DC3000: a model pathogen for probing disease susceptibility and hormone signaling in plants. Ann Rev Phytopathol **51**: 473–498

Yamada K, Yamaguchi K, Shirakawa T, Nakagami H, Mine A, Ishikawa K, Fujiwara M, Narusaka M, Narusaka Y, Ichimura K, et al. (2016) The Arabidopsis CERK1-associated kinase PBL27 connects chitin perception to MAPK activation. EMBO J **35**: 2468–2483

Yang Q, Guo J, Zeng H, Xu L, Xue J, Xiao S, Li JF (2021) The receptor-like cytoplasmic kinase CDG1 negatively regulates Arabidopsis pattern-triggered immunity and is involved in AvrRpm1-induced RIN4 phosphorylation. Plant Cell **33**: 1341–1360

Ye J, Fan J, Venneti S, Wan YW, Pawel BR, Zhang J, Finley LW, Lu C, Lindsten T, Cross JR, et al. (2014) Serine catabolism regulates mitochondrial redox control during hypoxia. Cancer Discov **4**: 1406–1417

You Q, Zhai K, Yang D, Yang W, Wu J, Liu J, Pan W, Wang J, Zhu X, Jian Y, et al. (2016) An E3 ubiquitin ligase-BAG protein module controls plant innate immunity and broad-spectrum disease resistance. Cell Host Microbe **20**: 758–769

Zhang W, Zhao F, Jiang L, Chen C, Wu L, Liu Z (2018) Different pathogen defense strategies in arabidopsis: more than pathogen recognition. Cells **7**: 252

Zhang Y, Sun K, Sandoval FJ, Santiago K, Roje S (2010) One-carbon metabolism in plants: characterization of a plastid serine hydroxymethyltransferase. Biochem J **430**: 97–105

Zhou H, Zhao J, Yang Y, Chen C, Liu Y, Jin X, Chen L, Li X, Deng XW, Schumaker KS, et al. (2012) Ubiquitin-specific protease16 modulates salt tolerance in Arabidopsis by regulating Na(+)/H(+) antiport activity and serine hydroxymethyltransferase stability. Plant Cell **24**: 5106–5122

Zhou X, Liao H, Chern M, Yin J, Chen Y, Wang J, Zhu X, Chen Z, Yuan C, Zhao W, et al. (2018) Loss of function of a rice TPR-domain RNA-binding protein confers broad-spectrum disease resistance. Proc Natl Acad Sci USA **115**: 3174–3179